ABSTRACT

Title of thesis: STUDYING WILDLAND FIRE SPREAD
                    USING STATIONARY BURNERS

                    Daniel Gorham, Master of Science, 2014

Thesis directed by: Professor Michael J. Gollner
                       Department of Fire Protection Engineering

Experiments were performed using stationary gas burners and liquid fuel-soaked wicks in order to characterize the flame geometry and buoyant instabilities present in stationary flames under inclined and forced flow configurations. These stationary flames revealed behavior similar to spreading wildland fires but offer an ideal platform to carefully study fundamental wildland fire behaviour such as reacting-flows instabilities that may play a critical role in fire spread.

Two types of flow conditions were used to perform experiments, a sloped fuel surface and forced-flow (wind aided) configuration. Small-scale inclined experiments were performed at the University of Maryland with liquid-fuel soaked wicks and large-scale experiments at the USDA Forest Service Missoula Fire Sciences Laboratory with a gas burner. These experiments were performed with over a range of heat-release rates and burner sizes for angles from 0 to 60 degrees from the horizontal. Forced-flow experiments were performed with gas burners in a large-scale wind tunnel at the Missoula Fire Sciences Laboratory and at the University of Maryland with a well characterized wind blower. These experiments were performed for a

range of heat-release rates and burner sizes in wind speeds from 0.2 to 3.0 ms^{-1}.

Flame geometry, such as centerline flame length and flame tilt angle were determined from high-speed side-view images. Flame intermittency and pulsations close to an inert surface were also measured using high-speed videography and arrays of micro-thermocouples. A method was developed to track the extension of the flame close to the surface which would come in direct contact with unburnt fuels ahead of the fire. These methods showed that the pulsation frequency is complex, however scaling over several orders of magnitude suggest large-scale coherent structures are present in the flow. Using peak frequencies measured, the stationary experiments follow a Strouhal-Froude scaling similar to flame pulsations in spreading fires and puffing pool fires.

Streamwise streaks were also observed and measured in the flow using high-speed videography. Streak spacing was observed to be associated with possible counter-rotating vortex structures in the fire. The spacing for streaks at the base of the flame for these stationary experiments appeared to be dependent on the incoming boundary-layer conditions and could possibly scale with the centerline flame length, similar to flame towers observed in spreading fires.

STUDYING WILDLAND FIRE SPREAD USING STATIONARY BURNERS

by

Daniel Gorham

Thesis submitted to the Faculty of the Graduate School of the
University of Maryland, College Park in partial fulfillment
of the requirements for the degree of
Master of Science
2014

Advisory Committee:
Professor Michael J. Gollner, Committee Chair
Professor Arnaud Trouvé
Dr. Mark Finney

Table of Contents

List of Figures

Nomenclature

c_p	Specific heat capacity (kJ/kg-K)
d	Burner depth (m)
D^*	Characteristic fire length
f	Flame pulsation frequency (Hz)
Fr	Froude number
g	Acceleration due to gravity, 9.81 (m/s^2)
G	Görtler number
H_f	Flame height (m)
L_f	Center-line flame length (m)
Q	Heat-release rate (kW)
Q'	Heat-release rate per unit depth, Q/d, (kW/m)
Q^*	Non-dimensional fire size
Re	Reynolds number
St	Strouhal number
T	Temperature (K)
U	Free-stream velocity (m/s)
w	Burner width (m)
x_a	Flame attachment length (m)
x_e	Flame extension length - location in attachment region (m)
x_f	Horizontal flame length (m)

Greek

δ	Boundary layer thickness (m)
ϕ	Flame tilt angle (deg)
θ	Slope angle (deg)
θ_m	Momentum thickness (m)
λ	Streak spacing (m)
ν	Kinematic viscosity
ρ	Density (kg/m^3)

Chapter 1:   Introduction

Wildland fire spread is often described as a function of three fire behavior components; fuel, weather, and topography. Since fire spread is essentially a series of ignitions, effects of fuels on spread are determined based on their propensity to ignite including loading, shape and size, compactness, continuity, and chemical content. Weather is the most variable component of fire behavior, changing in both time and space including atmospheric conditions such as temperature, relative humidity, stability, precipitation and wind speed. In contrast topography is relatively constant in time and only changes in space, such as elevation, aspect, land features, and steepness of slope.

There are several components that effect and contribute to fire behaviour. In the experiments performed here, wind speed and steepness of slope were independently investigated. Increasing the wind speed introduces fresh oxygen to burning fuels and can increase fire intensity as well as influence flame length and geometry. Increasing slopes can also have drastic effects on fire behavior, increasing intensities and flame length.

1.1 Motivation

Finney et al. [1] recently called for the development of a fundamental theory for wildfire spread. Current operational models used for predictions of fire spread are empirically based, while available "physically based" models lack a physical basis for the assumptions used to describe fuel particle ignition and fire spread. While computational power has increased, numerical tools for both operational firefighting and long-term predictions continue to rely on semi-empirical fire spread models primarily developed in the early 1970's. The lack of advancement in fundamental understanding of fire spread leads current models to be unreliable. Without a fundamental theory for fire spread, combustion, fluid dynamics, and heat transfer processes cannot be reliably applied to develop a truly physically based model.

Recent studies of spreading wind-driven fires in the 3×3 m wind tunnel at the USDA Forest Service, Missoula Fire Science Laboratory have shown coherent structures that form in the streamwise direction of the flow as well as spanwise fluctuations that propagate to the downstream edge of the flame zone contributing to intermittent fuel heating. The highly spatially-uniform fuel beds used in these experiments allowed for the observation of these structures with more repeatable results than previous efforts [2]. The results suggest that flame spread in fine fuel beds is driven by non-steady convective heating and intermittent flame contact on fuel particles. These heating characteristics were measured using micro thermocouple arrays and high speed video. The traveling flaming region and large experiment size, however, makes it difficult to carefully study these properties, for instance us-

ing a statistical analysis of these features which appear stochastically in the flow. A technique was therefore needed that could study these newly-observed instabilities and other general structures of propagating wildfires in a small-scale configuration that can be utilized over long times.

A stationary, non-spreading fire was chosen as it allows for a thorough statistical analysis of the flame structure. This technique has been used in the study of flame spread through the built environment before, however previous work focused on time-averaged properties of the flame, not intermittent effects important in spread through fine fuels [3]. Long-duration experiments allow for a large sample size and more control over variations in experimental parameters, such as decoupling of the heat-release rate of the fire from flow conditions, unachievable in spreading fires. The flame zone depth in the direction of fire spread can also be carefully adjusted via the size of the burner. High speed video and micro-thermocouples are useful with these fires to reveal and track buoyant instabilities in the fire flow which resemble those appearing in spatially-uniform fuel beds. The same intermittent heating observed in the fuel bed experiments were observed here with stationary burners, but with the ability to collect a larger data set. Observations made in these small-scale experiments can therefore be related to large-scale observed behavior. Other modifications to the flow field, such as the incoming boundary-layer thickness is also adaptable in these small-scale experiments.

1.2   Literature Review

1.2.1   Flame Geometry

Thomas [4] recognized a deficit in the research of fires exposed to the exterior environment in 1967 and presented some of the first engineering-based experimental and theoretical work on wildland fire spread. These experiments looked at spreading fires in both discrete and continuous fuel beds. His work supported the assumption of radiation dominated heating of unburned fuel ahead of the flame front, leading to flame spread. Thomas described the flame size as a dimensionless parameter, the ratio of flame length to burning region depth. Scaling analysis was used to determine the effect of external winds on flames, with the ratio of inertial forces from the wind and buoyant forces from the fire expressed as the Froude number

$$\text{Fr} = \frac{U^2}{gL_f} \tag{1.1}$$

This parameter is expressed in terms of the free-stream velocity U, gravitational acceleration g, and flame length L_f.

Motivated by a devastating escalator fire in King's Cross station, London, several investigators explored flame geometry for stationary burners in inclined trenches. Atkinson [5] performed experiments in an inclined trench to explore fire-induced flow for various configurations. He used a 10 x 27.6 cm gas burner built into a apparatus rotatable from 20 to 90 degrees. For angles less than 20 degrees the flow was plume dominated, and between 20 and 45 degrees buoyancy-driven flow

attached along an inert surface downstream of the burner, representing unignited fuel in a spreading fire. Smith [6] provides a qualitative relationship between the tilt angle (ϕ) of a flame and the slope angle (θ) of an inclined trench (Eq 1.2).

$$\phi_{vertical} = 2\theta. \tag{1.2}$$

This relationship is based on a mass balance of air on the upstream and downstream side of the flame.

Several other investigators [5–9] have explored the effect of side walls on inclined fires and their effect on flame geometry, later defined as the trench effect. The plume geometry in non-trench inclined fires have also been investigated in orientations from pool to ceiling fires [10, 11].

Oka et al. explored the effects of cross-wind on an unconfined, stationary fire geometry. Their experiments included the use of a square propane burner with fire sizes ranging from 0.75 to 16 kW in cross-wind velocities of 0.5 to 4.0 m/s [12]. Experiments were performed for two surface conditions, "with floor," where there was a 1.2 m long flat plate extending from the outlet of the blower to the burner surface and "without floor," where this false floor was removed. These essentially created two inlet flow conditions, one with a developed boundary layer and another with a uniform incoming flow. The effects of burner aspect ratios on the flame geometry was also measured, using luminosity from cameras to determine the average flame shape and two-dimensional thermocouple arrays for isothermal curves [13]. Based on their results, the authors proposed that the flame tilt angle

can be determined using a ratio of mass fluxes, between the upward mass flux from the fuel and the mass flux of air from the cross-wind. The balance is written as a ratio of the Froude number and the non-dimensional fire size, Q^*,

$$\frac{H_f}{d} = \frac{\text{Fr}^{2/3}}{Q^*} \tag{1.3}$$

where H_f is the flame height and d in the burner depth.

1.2.2 Flame Pulsation

A review of pulsations observed in diffusion flames, especially pool fires was presented by Malalasekera et al. [14]. The authors described the mechanism of flame oscillations in pool fires as three steps; formation of a torodial vortical structure due to acceleration of buoyant gases, contraction of the flame near the base of the flame as the vortex rises, and accumulation of buoyant gas to return to the base flame structure.

Several investigators have previously explored using a Strouhal-Froude relationship to scale the flame pulsation frequency of pool fires [15]. The Strouhal number is a non-dimensional representation of the oscillations in a flow,

$$\text{St} = \frac{f L_f}{U} \tag{1.4}$$

where f is the characteristic frequency, L_f is the characteristic length, and U is the characteristic velocity [16].

More recently, Finney et al. [2,17] used Strouhal-Froude scaling to understand

the flame pulsations in laboratory-scale spreading wildfire experiments. They used a frequency obtained from micro-thermocouples based on level-crossing of the gas-phase flame temperature. The flame length and free-stream wind speed were used as the characteristic length and velocity respectively.

1.2.3 Streamwise Streaks

Vortex structures have also been observed in laboratory and field observations of wildfires [18]. Streamwise streaks in the burned fuel were observed in spreading fire experiments, and observed flame towers were measured and correlated with flame length [2]. The structures resemble counter-rotating vortex pairs (Taylor-Görlter vortices) which are known to form over concave surface [19]. Boundary layer effects on the vortex formation were initially investigated [20] which lead to a multi-mechanism instability approach to understanding.

Several investigators observed streamwise streaks in small inclined experiments [21–23]. In these experiments a metal plate submerged in water was heated to induce natural convection and slightly inclined. Investigators observed "secondary-flows" which were seen as streamwise streaks, analogous to Görtler vortices. Streaks present in wall-bounded turbulent boundary layer flows have also been observed [24].

1.3 Research Objectives

The objective of this thesis is to study flame structure and instabilities on stationary fires to better understand these features occurring at large scale in the hope

of translating that knowledge to the development of a fundamental understanding of wildland fire spread. Experiments were performed in inclined and forced-flow configurations, two of the most important conditions in wildfire spread. Several fuel sources were used, including variations in liquid fuel type and gas burner size.

The flame geometry has been shown to be an important factor for understanding fire spread. Important parameters such as the flame length, flame height and tilt angle were measured for these experiments. Determining the effects of flow conditions on flame geometry and the potential for flame contact to unignited fuels will lead to a better understanding of particle heating in wildfire spread.

Flame pulsations ahead of the flame front can also cause intermittent flame contact and heating of fuel particles, leading to ignition. Direct flame contact on the fuel particles causes conductive and convective heating and convective cooling, forming a non-steady particle ignition process for fine, discrete fuels. The frequency of flame pulsations and the distance ahead of the flame front these pulsations travel were measured to better understand their underlying mechanisms. Coherent structures and instabilities observed in the flow are suspected to be responsible for the pulsating phenomena. Studying this behavior in small-scale experiments is vital to characterize the mechanics responsible for spreading from small to large scales.

Chapter 2:   Experimental Setup

2.1   Small-Scale Inclined Experiments

Initial experiments were performed using a small-scale inclined apparatus with liquid-fuel soaked wicks at the University of Maryland. These experiments were performed first to determine if using stationary burners and image analysis was a valid way to observe instabilities. The steady burning rate of these inclined fuel wicks was also measured to determine the effect of slope angle and burner aspect-ratio on the burning rate of the fuel.

The experimental apparatus used was adapted from a previous study on inclined flame spread over solid fuels [11]. The apparatus consisted of a base plate with two vertical supports, and aluminum plate connected in a fashion so it is rotatable 360 degrees (Figure 2.1). The rotatable surface was a $22 \times 60.5 \times 0.3$ cm aluminum plate. Non-combustible insulation board was used as an inert surface around a fuel-soaked wick. This single sheet of insulation board, 60×40 cm was Superwool brand High-Temperature Board SB with a rated temperature of $1150°$C and a density of 360 kg/m^3.

A slot for the fuel-soaked wick was cut into the insulation board 5 cm from the bottom and 5 cm from each side (Figure 2.1). This was done both to reduce the
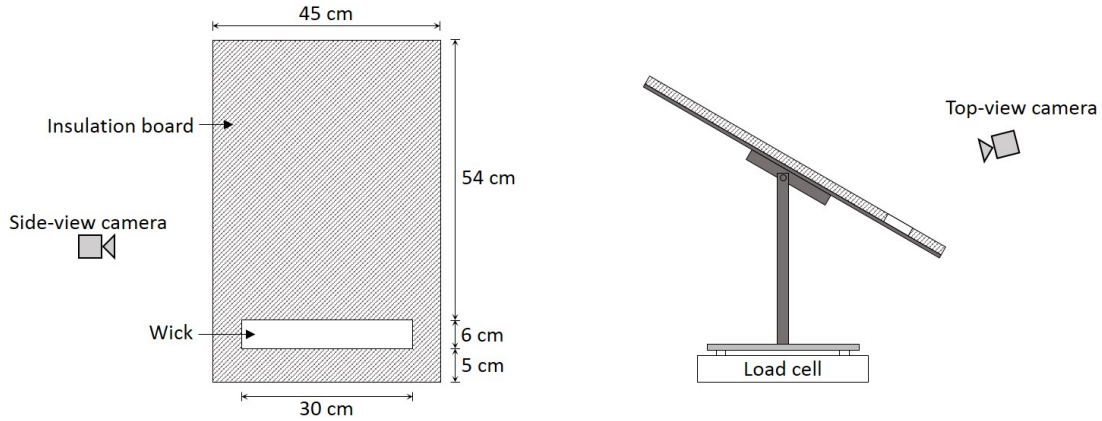
Figure 2.1: Diagram of experimental setup used for inclined experiments at UMD.

effects of side air entrainment and downstream of the wick, provide an attachment surface, acting as the surface where unburned fuels would be during simulated flame spread.

The same insulation board was used to make the liquid fuel burners. The wicks measured 30 cm in width and three depths were used: 3, 6, and 12 cm. After the insulation was cut to size for the desired wick, it was exposed to a propane torch for 10-15 minutes to burn off any residual binders from the manufacturing processing. It also made the insulation more porous so it could absorb more fuel. The bottom and sides of the wick were covered with aluminum foil leaving only the top surface expose, preventing liquid fuel from leaking out of the bottom or sides of the wick when inclined.

The burning rate was determined based on the mass-loss rate of the burning fuel. A Metler-Tolledo MS32001L load cell was used to measure the instantaneous mass of the fuel sample at 1 Hz with a precision of 0.1 grams. The balance was

10

connected to a computer via USB cable and data was logged using Balance Link software. Various liquid fuels with different properties were used for these experiments to achieve a range of fire sizes including methanol, ethanol, acetone, and heptane.

The amount of fuel used was based based on the size of the wick and volume required for total saturation. The volume of fuel used for 3, 6, and 12 cm deep wicks was 60, 120, and 180 mL respectively. The same amount of fuel was distributed evenly on the wick surface with a liquid syringe for each of the experimental configurations.

Side-view images were taken with multiple cameras including a Canon SLR and a Casio EX-F1. To capture a two-dimensional image of the flame the camera was mounted on a tripod and rotated to the same angle as the apparatus. Images were capture continuously with the Canon SLR at 3 frames per second (fps) and in high speed with the Casio EX-F1 at 300 fps. The SLR images were high-resolution, at 6000×4000 pixels while high speed video was recorded at 528×312 pixels. Top-view images were also taken with both the Canon and Casio cameras.

Before each experiment, any residual soot from previous experiments was burned off the wick with a propane torch for 3 to 5 minutes. While the wick was allowed to cool, the apparatus was rotated to the desired angle, which was measured using a digital inclinometer. The side-view camera was manually focused on the middle of the top surface of the insulation board. The top-view camera was setup on a tripod behind apparatus as approximately at 45 degree angle measured from the surface of the insulation board. The camera was manually focused on the

wick and downstream inert surface. Once cool, the fuel wick was fully saturated with liquid fuel using a syringe, and then placed into its slot in the insulation board. Mass data began being recorded on the computer connected to the load cell. The lights were turned off and the cameras turned on. The wick was ignited with a lighter, being careful not to touch the surface disturbing the mass data.

2.2 Large-scale Inclined

Based on successful observation of large-scale fire features with the small-scale experiments at UMD, large-scale experiments were performed at the USDA Forest Service Missoula Fire Sciences Laboratory. Here, a large 1.81 m × 0.61 m flame wall designed by Jimenez et al. [25] was retrofitted for inclined experiments. A gearbox and crank were added to the rotation system to allow the wall to be held at an angle between 0 and 90 degrees (horizontal and vertical). An extension at the top of the burner was built for the inert attachment surface.

To achieve an even, uniform gas flow at the burner surface, a three layer diffusion medium was used. An interior layer of 0.06 cm thick fiberglass cloth, followed by a layer of fiberglass batting, and finally a 2.5 cm thick sheet of ceramic foam made up the burner surface. The porosity of the top layer of Cotronic ceramic foam was 17.7 pores per centimeter. The exposed burner surface area was 0.61 meters wide and 1.83 meters long. To produce a line fire, a large section of the burner was sealed so that gas flowed only out of the exposed ceramic surface. A 1.5 m long steel sheet covered the bottom portion of the burner (Figure 2.2) and
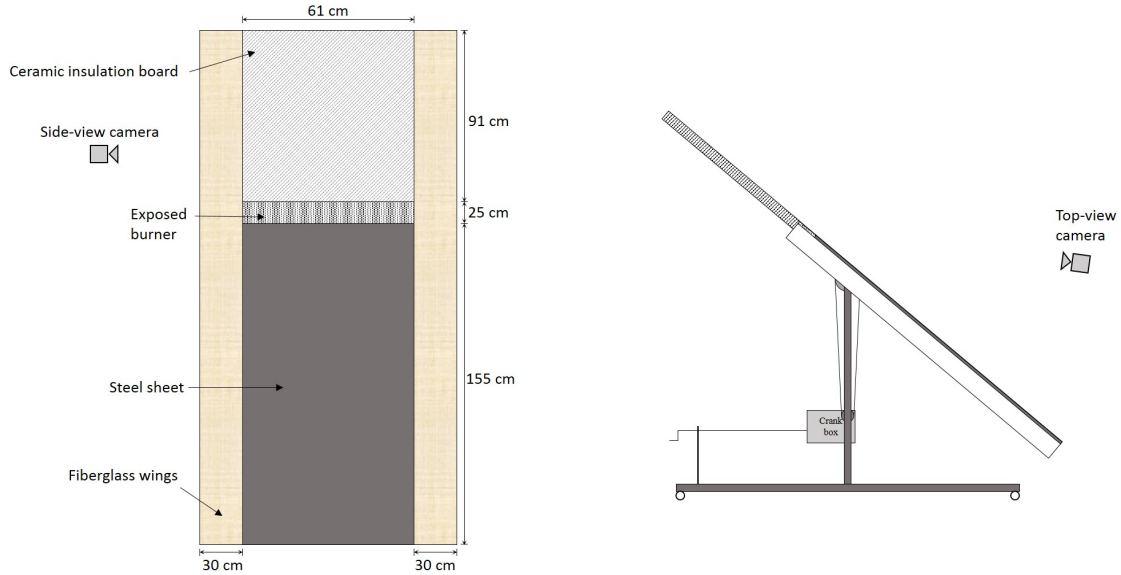
Figure 2.2: Diagram of the experimental setup for large-scale inclined experiments at the Missoula Fire Sciences Laboratory, (left) topview and (right) sideview.

was sealed around the edges with aluminum tape. The remaining 0.33 m could be sealed with aluminum foil and insulation to change the exposed burner area. The burner width was always 0.61 m wide, and experiments were performed at depths of 6.4, 12.7, and 25.4 cm.

The fuel used in the burner was ethylene gas, chosen to reduce buoyant effects in the burner plenum because its molecular weight is close to that of air, 28.05 g/mol versus 28.96 g/mol for ethylene and air respectively. Gas flow into the burner was controlled with an Omega mass flow controller. Experiments were performed using ethylene gas flow rates of 39.1, 78.1, 156.3, and 234.6 lpm corresponding to fire sizes of 38.6, 77.1, 154.3, and 231.6 kW, respectively.

The side-view camera used for these experiments was a Phantom model high-

speed camera with a fish-eye lens recording at 120 fps at a resolution of 1920×1200 pixels. Due to the length of the flame wall, both the burner and inert surface were very high so that the side-view camera needed to be mounted on a tripod capable of reaching 9 feet. The camera was rotated on the tripod to be at the same angle as the burner and inert surface on the apparatus. The camera was focused on the top edge of the inert surface. The fish-eye lens allowed for a wide range to be captured past the leading edge of the burner, however corrections were made via comparison with ruler measurements to minimize and distortion effects from the lens. Side-view videos were only recorded for a 10 second duration for each test using the Phantom camera because of memory limitations.

The top-view camera was a Casio EX-FH25 recording at 120 fps at a resolution of 640×480 pixels. In order to maintain a consistent viewing angle on the flame while the flame wall was rotated to higher slope angle, the tripod was mounted to the bottom of the flame wall. This allowed for the top-view camera to remain focused on the same portion of the flame without making adjustments when the flame wall was rotated.

An array of micro-thermocouples were used to measure temperature fluctuations downstream of the burner. The thermocouples were Omega brand K-type, with bead diameter of 12 microns. The thermocouple array consisted of 52 probes mounted in a wire holder 1 cm above the inert surface, with the first thermocouple 5 cm downstream of the burner and subsequent thermocouples spaced 2 cm downstream. A National Instruments data logger was used to record temperature signals from all thermocouples at 120 Hz.

Figure 2.3: Picture of experimental setup for large-scale inclined experiments with modified flame wall.

A picture of the experimental setup during a test is shown in Figure 2.3. The wall is shown rotated to a desired slope angle, measured by a digital angle finder. A side-view camera was placed on its tripod and focused on the top surface of the inert insulation board. The top-view camera was mounted on the tripod, which maintained an orientation angle with the burner. Before tests, the burner was first purged with nitrogen gas and then ethylene fuel was injected through the mass flow controller. Once the flame was ignited with a propane torch the nitrogen was turned off and the plenum allowed enough time to be cleared of any remaining nitrogen. The lights in the combustion chamber were turned off and the cameras began recording, as well as the thermocouple data acquisition. After each experiment the apparatus was rotated back to the horizontal position and the burner purged with nitrogen to burn any remaining fuel.

2.3   Missoula Forced-Flow

While working as a visiting researcher at the fire lab in Missoula, initial forced-flow experiments with a stationary burner were performed in the same wind tunnel used for large spreading fire experiments. The initial prototype for the flame wall, a 30×25 cm sintered metal burner was used as the burner, and an apparatus for holding the ceramic insulation board was built flush with the burner surface.

The wind tunnel used had a cross-sectional area of 3×3 meters. The wind speed was measured with a velocity probe in the centerline of the wind tunnel, and experiments were performed at wind speeds of 0.22, 0.44, 0.67, 0.89, 1.11, and 1.34

m/s.

Cotronics high-temperature ceramic insulation board was placed flush with the burner surface, providing an inert surface for experiments and limiting side-air entrainment. The top surface of the burner and inert insulation was approximately 30 cm above the floor of the wind tunnel, putting it directly into the free-stream flow. A diagram of the experimental setup is show in Figure 2.4. Propane gas was used in the burner for all forced-flow experiments. The fuel flow rate was measured with a volumetric flow meter and experiments were conducted at flow rates of 9, 13, and 18 lpm corresponding to fire sizes of 7.5, 10.9, and 15.1 kW.

The same Phantom camera described earlier was used to record side-view video. The camera was mounted on a tripod outside of the wind tunnel, level with the top of the burner and inert surface of the apparatus. The camera had a clear line-of-sight of the apparatus in the wind tunnel through an observation window. Despite the tripod shown in the photograph, top-view images were not captured for the wind tunnel experiments at Missoula because of difficulties avoiding disturbing the flow when mounting the camera. A picture of the experimental setup in the wind tunnel is shown in Figure 2.5.

Forced-flow experiments were performed in the Missoula wind tunnel over the course of a week, with all of experiments for one fire size completed straight-through (all completed in the same day). The experiments at 4.3 kW were completed first, and then the apparatus had to be removed from the wind tunnel for other experiments. The next time the apparatus was put in the wind tunnel, the experiments for fire sizes 6.3 and 8.7 kW were completed in succession without removing the
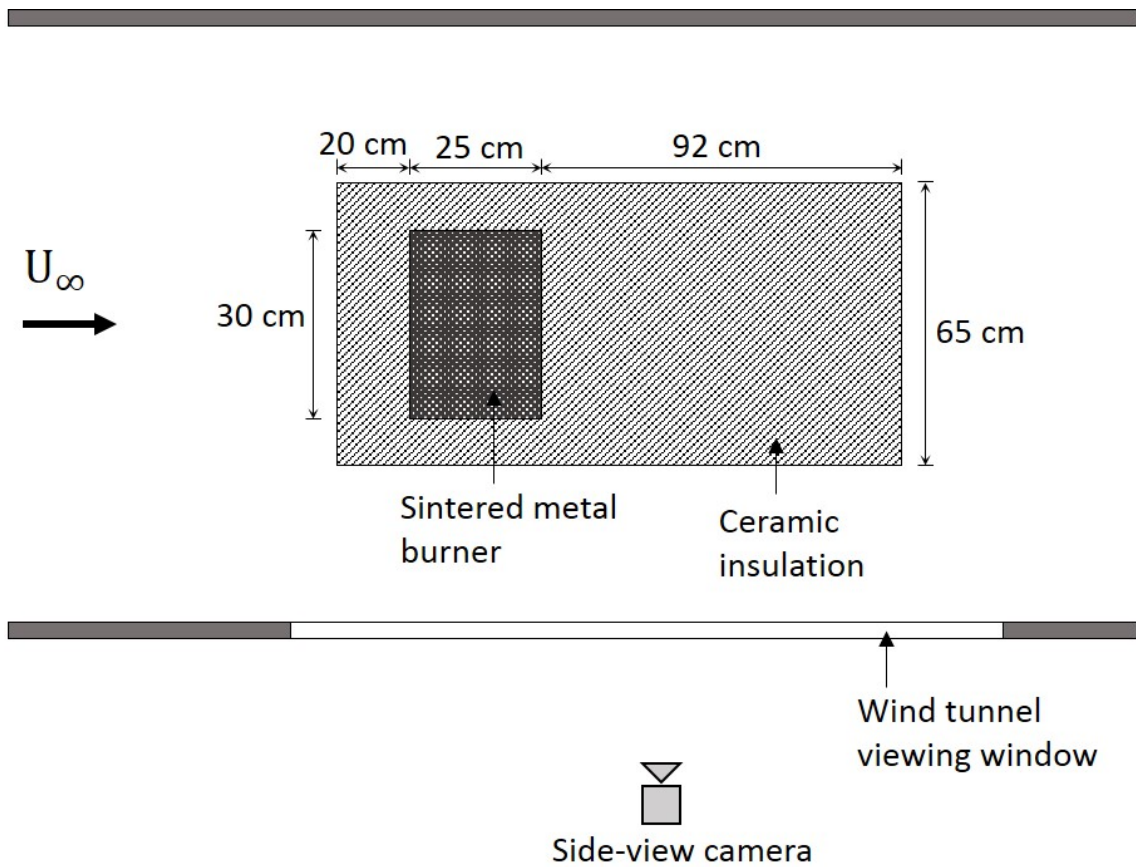
Figure 2.4: Top-view diagram of forced-flow experimental setup performed in the wind tunnel at the Missoula Fire Lab.

Figure 2.5: Photograph of the forced-flow experimental setup performed in the wind tunnel at the Missoula Fire Lab. In this view, the wind is blowing toward the photographer.

apparatus from the wind tunnel again.

2.4 UMD Forced-flow

After successfully acquiring results using the stationary burner in the Missoula wind tunnel, smaller, more detailed forced-flow experiments were performed at the University of Maryland using both liquid and gaseous fuels with a specially-built uniform velocity wind blower for combustion experiments. Design and characteristic of the wind blower are discussed in Section 2.4.1. Some initial experiments were performed with heptane soaked fuel wicks to determine the effect of the incoming boundary layer across the flat surface while later, sand burners were designed and used for testing with gaseous fuels.

The forced-flow experiments with the liquid fuel wicks used the same apparatus as in small-scale inclined experiments, but with the apparatus parallel with the floor (a slope angle of 0°). Two wick sizes were used, 6 and 12 cm deep in the flow direction, both 30 cm wide. The wicks were fully saturated with heptane in the same manner described previously.

Several sand burners were designed and built, including two iterations and three different burner dimensions. The first burner was made with 1/32 inch (0.07 cm) thick galvanized steel with a burner surface of 25.4 × 4.54 cm. The burner was 6.5 cm tall with a 2 cm tall plenum, and 4.5 cm of fine sand. Propane fuel entered a 1/4 inch (0.6 cm) NPT bulkhead fitting on the bottom side of the burner and filled the plenum. The sand was supported above the plenum with a mesh screen which

also acted as a diffuser to evenly distribute mass flux of gas fuel from the top of the burner.

After intial testing with the fuel wicks and the first generation sand burner, two design additional sand burners were designed and built. Both burners were made of 1/8 inch (0.3 cm) thick stainless steel, bent and and welded to form the burner walls. The burners were both 8 cm tall and 25 cm wide, measured on the inside. One burner was 5 cm deep in the flow direction while the other was 10.6 cm. A 1/4 inch (0.6 cm) NPT connector was bored through the bottom side of the burner and welded in place. The plenum on both burners was approximately 2 cm and the same sand was use to diffuse the gas, 6 cm deep on these burners.

All three sand burners were operated with propane fuel. The mass flow rate of propane gas was controlled with an Alicat MCR-100SLPM-D mass flow controller. Experiments were conducted with fuel flow rates of 4.9, 6.6, 10, and 15 lpm corresponding to fire sizes of 2.3, 3.2, 4.8,and 7.2 kW, respectively. A diagram of the experimental apparatus is shown in Figure 2.6. The free-stream velocity was controlled by the power of the blower. Experiments were performed at wind speeds ranging from 0.6 to 2.7 m/s.

Two side-view cameras were used for these experiments. High-speed and high-definition video was taken with a Casio EX-F1 digital camera. The high-speed video was taken at 300 fps at 512×384 pixel resolution. The same camera was used for high-definition video at 60 frames-per-second at 1920×1080 pixel resolution. A Nikon D7100 DSLR camera was also used for continuous shooting of side-view images at 6 frames-per-second. At high-resolution, top-view camera images were
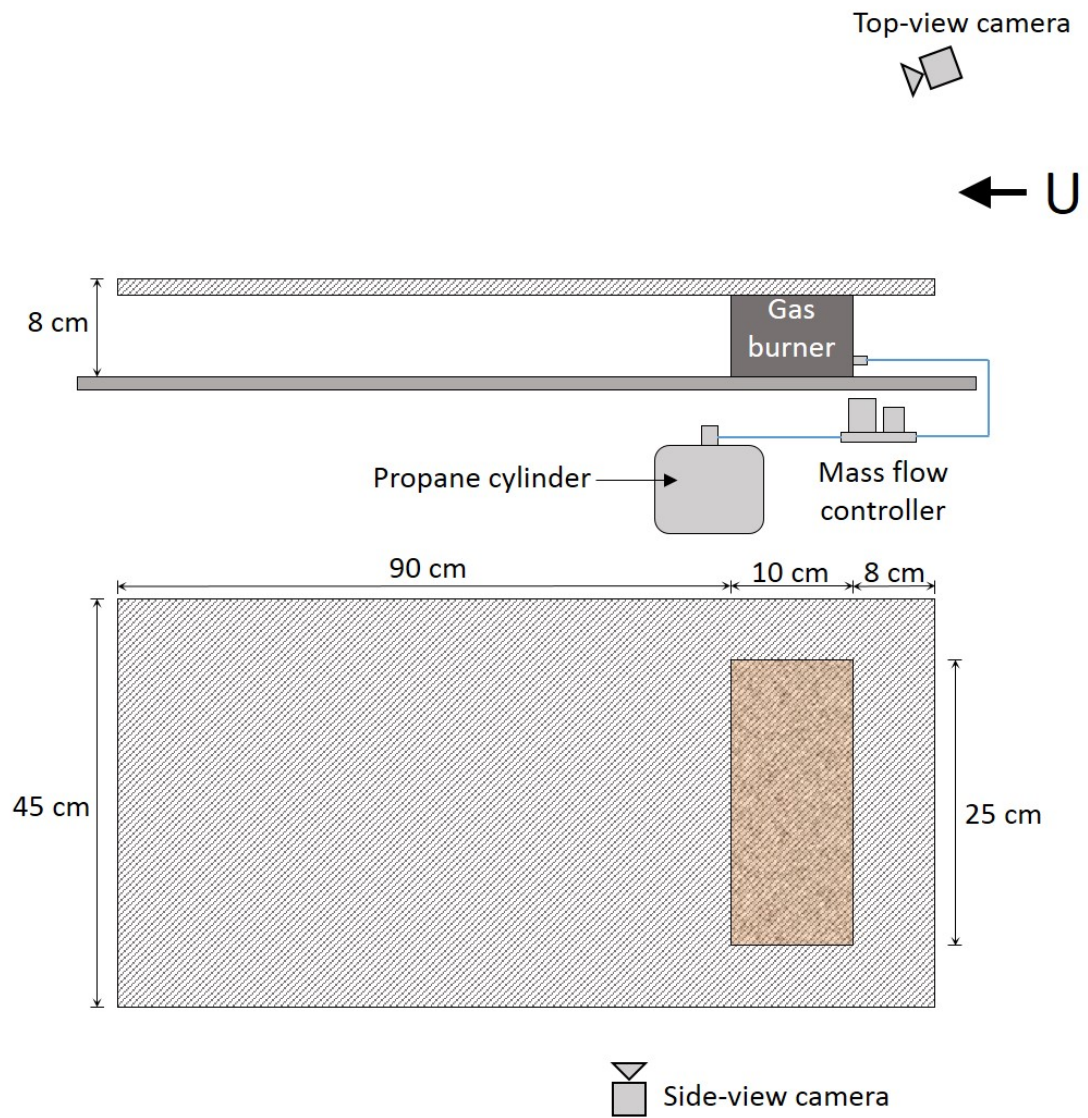
Figure 2.6: Diagram of the forced-flow experimental setup at UMD.

Figure 2.7: Picture of the forced-flow experimental setup at UMD.

taken with the previously-described Canon SLR.

A picture of the experimental setup is shown in Figure 2.7. The apparatus was setup at the outlet of the blower exhaust and the propane cylinder and mass-flow controller connected to the burner. A side-view camera was setup to be focused on the top of the inert surface and the top-view camera focused on the burner and the downstream surface.

To begin testing the blower was plugged in and turned on to the desired velocity, which was measured in the free-stream with an Omega hot wire anemometer. The fuel flow rate out of the gas burner was set on the mass-flow controller and the burner ignited with a propane torch. The lights in the room were shut off and cameras began recording. Experiments were run for 30 seconds after which the cameras were shut off and exhaust hood was turned on.

2.4.1   Wind blower design

Forced-flow combustion experiments are difficult to conduct in traditional wind tunnels for several reasons. In recirculating wind tunnels the makeup air is contaminated with by-products of combustion and can effect the combustion efficiency at the fire source. Many large wind tunnels are constructed of non-fire resistant materials and would become overwhelmed by moderately sized fires in the test chamber. A solution was to design and build a wind blower, where a uniform-velocity flow field can be blown onto a fire and exhausted in a fire hood similar to ambient fire experiments.
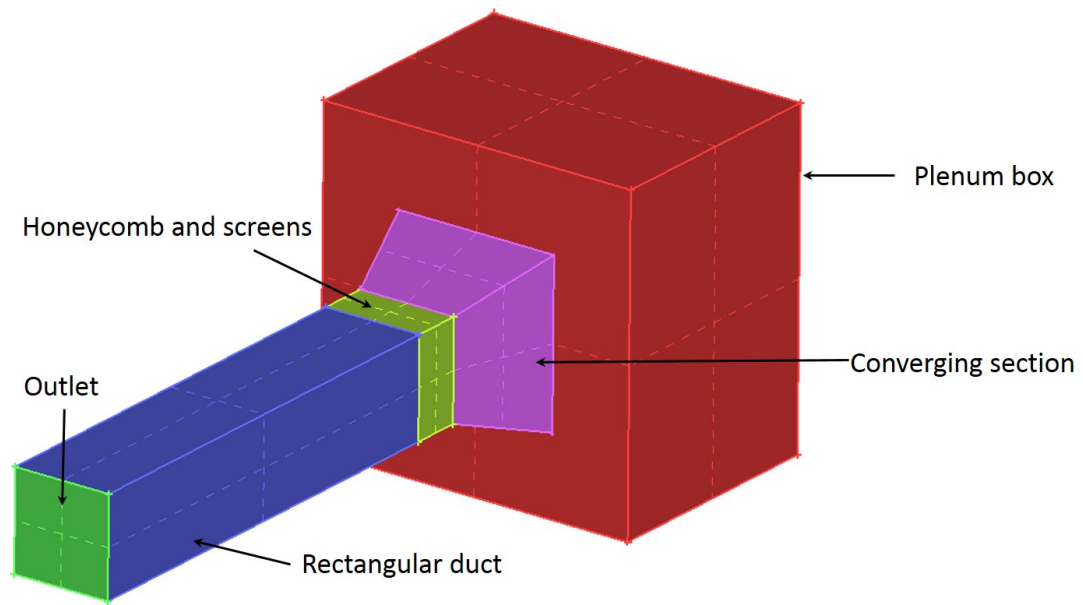
Figure 2.8: Design and components of a uniform blower built at UMD for forced-flow experiments.

A uniform velocity wind blower was designed and constructed at the University of Maryland to conduct these forced-flow fire experiments. The wind-blower design consists of a centrifugal fan that pressurizes a large plenum and then contracts the air through a mesh screen and flow-straightening honeycomb before traveling through a 1.3 m long straight exhaust duct shown in Fig. 2.8.

The centrifugal fan was an EBM Papst Nautilair combustion blower controlled via pulse-width modulation capable of max flow rate of 1200 cfm. The pulse-width modulation allowed the blower speed to be controlled without causing oscillations in the flow. The plenum box, converging section, and exhaust duct were all constructed out of of 1/2 inch (1.27 cm) thick plywood sheets. The dimensions of these
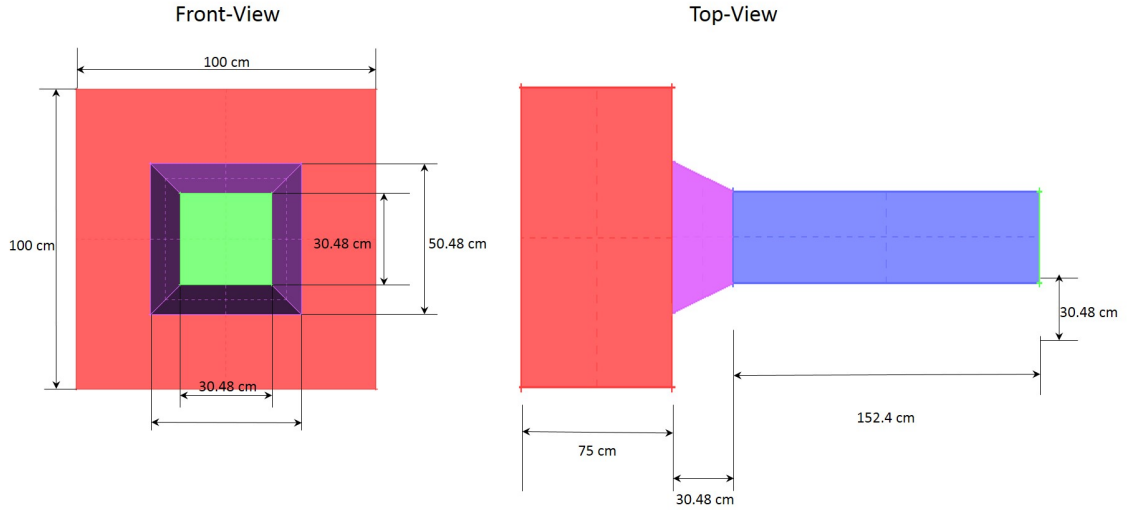
Figure 2.9: Top and front view diagram of wind-blower with dimensions.

components are shown in Figure 2.9. The plenum box was built as a 5-sided cube permanently connected, with the 6th side being the front where the converging section is connected and can be removed to transport the wind-blower and access the inside. The front side is connected by cinching it with angle brackets and sealing the connection with foam tape. The converging section was connected to the plenum box with angle brackets and sealed with silicon sealant. The final piece of the blower was the exhaust duct. The duct was connect to the converging section and sealed with duct tape. Approximately 5 cm into the exhaust duct was a mesh screen to promote mixing of the flow, followed by a 1/2 inch (1.27 cm) thick honeycomb flow straightener. The flow finally traveled approximately 0.9 m through the duct, reaching the exhaust exit, where a nearly uniform-laminar flow field was blown over a test region.

The flow field at the outlet of the wind blower was measured with a Dantec

26

Dynamics hot-wire anemometer system. The hot-wire was connected to a two-dimensional Velmex traverse system to characterize the flow field. A vertical centerline velocity profile was measured with a spatial resolution of 1 mm for four different. At each point the velocity was sampled at 50 kHz for 10 seconds. The velocity profiles at the outlet of the exhaust duct are shown in Figure 2.10 for free-stream velocities of 0.56, 0.99, 1.55, and 2.07 m/s. The boundary-layer thickness for all four of the velocities was approximately 27 mm. Velocity profiles were also measured at distances downstream of the exhaust outlet. Figure 2.11 shows the velocity profiles at the leading edge of the burner and 8 cm downstream from the exhaust outlet. The boundary layer thickness was found to increase as the velocity increases, opposite to the Blasius boundary layer theory for a flat plate, something that will continue to be investigated further.
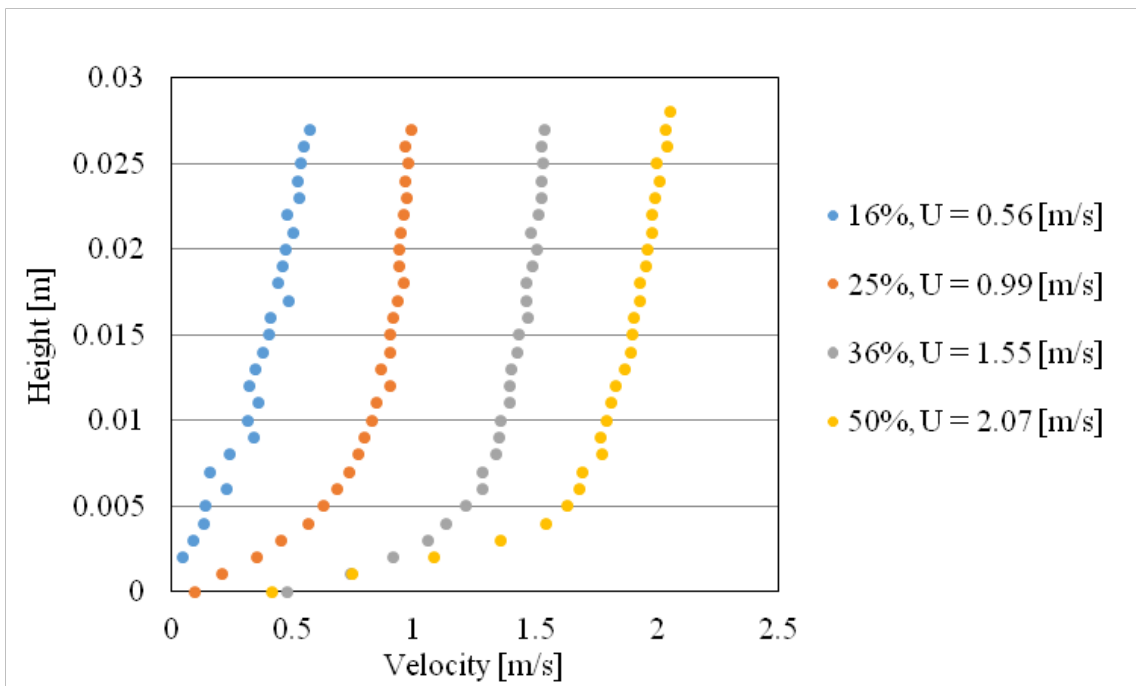
Figure 2.10: Velocity profiles measured at the outlet of the exhaust duct for different blower capacities (%) and free-stream velocities (U, m/s).
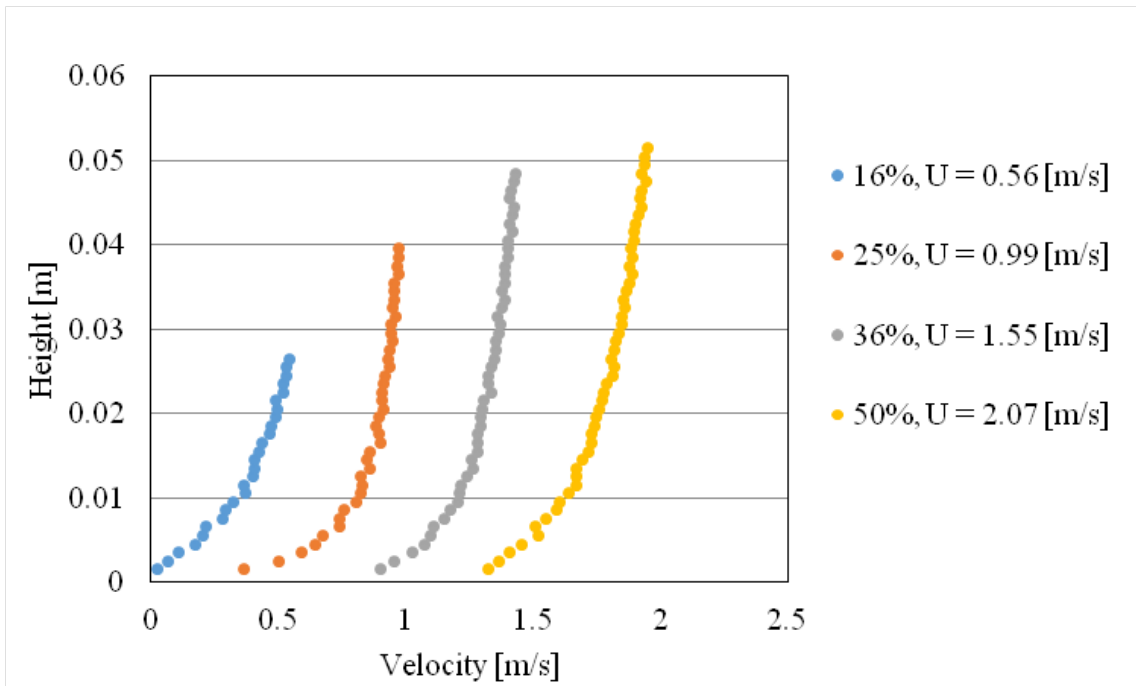
Figure 2.11: Velocity profiles above burner, located 8 cm downstream from the exhaust outlet are presented for different blower capacities (%) and free-stream velocities, U (m/s). The insulation board is connected flush to the blower outlet.

Chapter 3: Results

3.1 Flame Geometry

Knowledge of the mean flame geometry, such as flame length, tilt angle, etc. is useful for understanding fire behavior and can be easily obtained from stationary fire experiments. Experiments were performed for both horizontal forced-flow and inclined configurations for both liquid and gas fuel burners. Two-dimensional flame geometry measurements were taken from the side-view images of experiments. Flame geometry measurements included the center-line flame length (L_f), flame height (H_f), horizontal flame length (x_f), flame tilt angle (ϕ), and the flame attachment length (x_a) (Figure 3.1). Measurements were taken based on the average flame tip, which is defined as the furthest downstream point, that when connected to the mid-burner point, approximately cut the flame in half. The flame tip location and other relevant parameters were measured via MATLAB's user-input interface.

To determine the distinction between flame and non-flame in recorded images, a representative light-intensity threshold was used to convert the images, to binary black and white images where white pixels represented flame and black represented non-flame. A MATLAB function *thresh_tool* was used to determine the light-intensity threshold level for images from an experiment. Once the experimen-
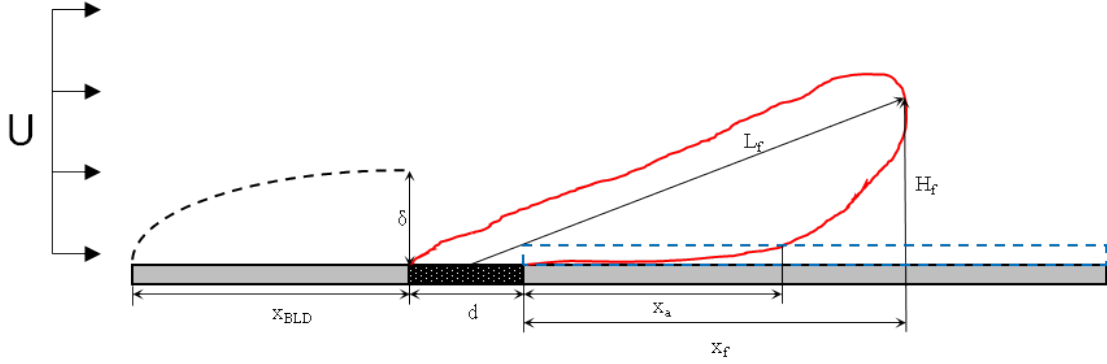
Figure 3.1: Simple two-dimensional geometry diagram for a wind-blown flame.

tal video was loaded into MATLAB, the *thresh_tool* function was run on a random image and the threshold level determined from user input. The level was selected based on the highest value with no error in interpreting flame from non-flame. The average of five threshold levels from random images in a single test were averaged and this value was used for all images in the experiment.

Thresholding converted the gray-scale images to binary, black-and-white images, with 1 indicating flame and 0 indicating no flame. The average image is the sum of all the binary matrices, divided by the number of images. This average image contains the same number of pixels as all of the individual images, with each having a value between 0 and 1, essentially representing the percentage of time the flame was at that pixel location. With this "flame probability" image, the average flame shape based on a 50% probability, following the methodology used by Audoin et al. for pool fires [26]. A range of pixel values was used, 0.48 to 0.50, to determine the average flame location. The binary average image was converted in a RGB image, and those pixels that fell within the range of 0.48 to 0.50 were colored red to denote

Figure 3.2: Flame averaging process based on image luminosity. (a) Still image from experiment video (b) black-and-white image converted using average threshold and (c) averaged image with average flame geometry represented by red pixels.

the average flame geometry (Figure 3.2).

Flame height and horizontal flame length were vertical and horizontal measurements respectively from the downstream edge of the burner to the flame tip. The flame length was a straight line between the mid-burner point and flame tip. The flame tilt angle, ϕ, is defined as the angle between the centerline flame length and the fuel surface. It can be determined by finding the inverse tangent of the flame height, H_f and the horizontal flame length, x_f plus half the burner depth, $d/2$,

$$\phi = \arctan\left(\frac{H_f}{x_f + d/2}\right). \tag{3.1}$$

It can also be important to understand the length along the surface a flame extends forward of the pyrolyzing zone, making up the pre-heating length for convectively-spreading fires. Flame attachment, x_a, is defined as the horizontal flame length in the region of interest close to the surface.

32
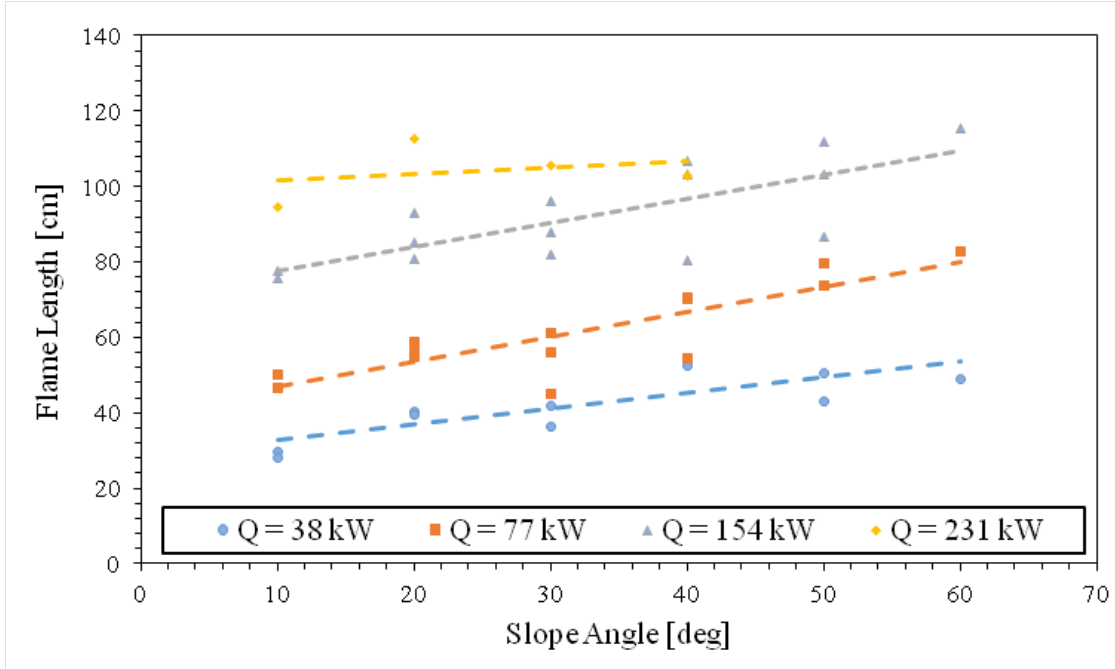
Figure 3.3: Flame length, L_f, versus the slope angle, θ, of large-scale inclined experiments for different fire sizes.

3.1.1 Inclined Experiments

Measurements of flame geometry from large-scale inclined experiments are shown below. Several experiments were performed for each set of experimental conditions (burner depth, fire size, and slope angle) the results were averaged for that data point. Figure 3.3 shows how the centerline flame length, L_f, increases fairly linearly with increasing slope angle of the experimental apparatus. The flame length attaches to the surface as it approaches the vertical orientation and flow is similar to wall fire configurations. Longer flame lengths increase the flame extension and convective heating of unburned fuels.

Figure 3.4 shows how the flame height, H_f decreases as the slope angle in-
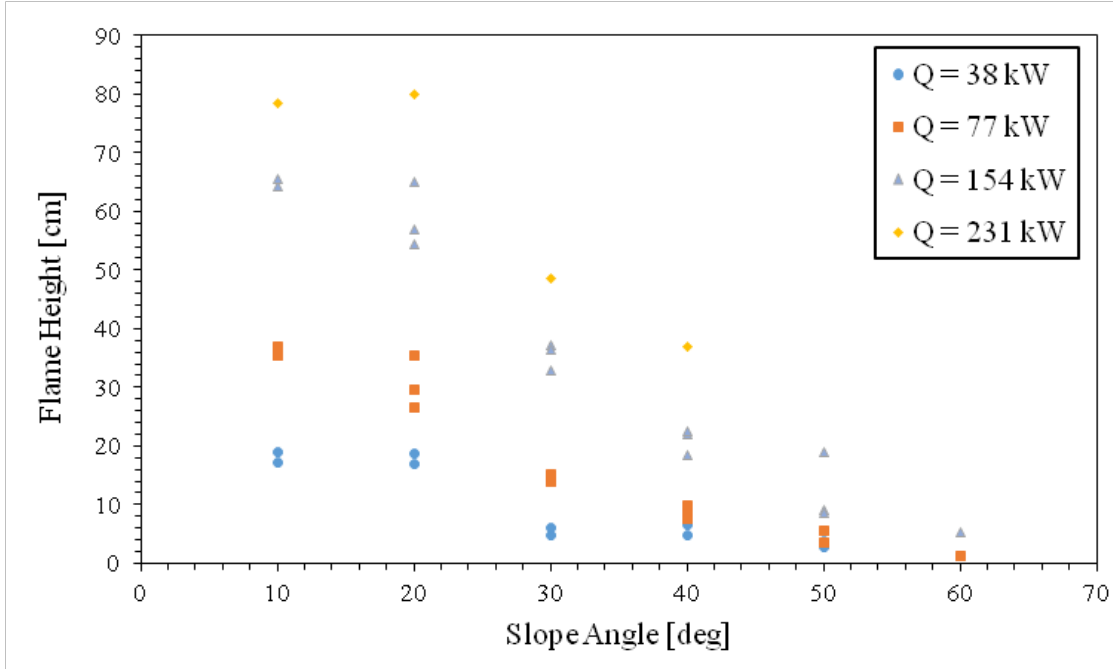
Figure 3.4: Flame height, H_f, versus the slope angle, θ, of large-scale inclined experiments for different fire sizes.

creases. This is expected as the flame attaches more to the surface as the slope moves toward a vertical wall fire. For all fire sizes, flame height is approximately the same for 10 and 20 degree slope angles, but decreases at slope angles above 30 degrees. This is in agreement with the transition between a plume fire to an attached fire. Figure 3.5 shows the average flame geometry of two large-scale inclined experiments, both with a burner depth of 12.7 cm and fire size of 154 kW. The image on the left is at a slope angle of 20 degrees where the flame forms a plume like shape rising sharply from the downstream surface, and the image on the right is at a slope angle of 40 degrees, where the flame geometry is more attached to the downstream surface.
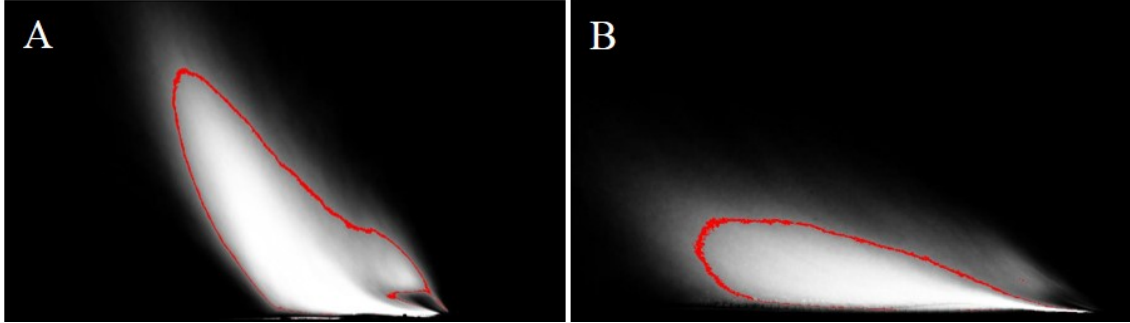
Figure 3.5: Average flame images from two inclined experiments, both with burner depth = 12.7 cm and fire size = 154 kW. (a) The slope angle is 20 degrees and the flame geometry rises sharply above the downstream surface like a plume (b) The slope angle is 40 degrees and the flame geometry follows the downstream surface like it is attached.

Figure 3.6 shows the horizontal flame length, x_f, which increases as the slope angle increases, similar to L_f. The horizontal flame length influences radiative heating of unburned fuels ahead of the flame front.

Figure 3.7 shows the flame angle, ϕ, which decreases as the slope angle increases. An exponential relationship between the flame angle and the slope angle could be a factor of the transition from a plume fire to an attached flame. The slope angle also increases slightly as the fire size increases for the same slope angle, so for larger fires the flame angle is less sensitive to the slope angle.

3.1.2 Forced-flow Experiments

Results from flame geometry measurements of forced-flow experiments from both the Missoula wind tunnel and the UMD wind blower are shown in Figures 3.8 - 3.11. This data is compiled from experiments performed in the Missoula wind tunnel
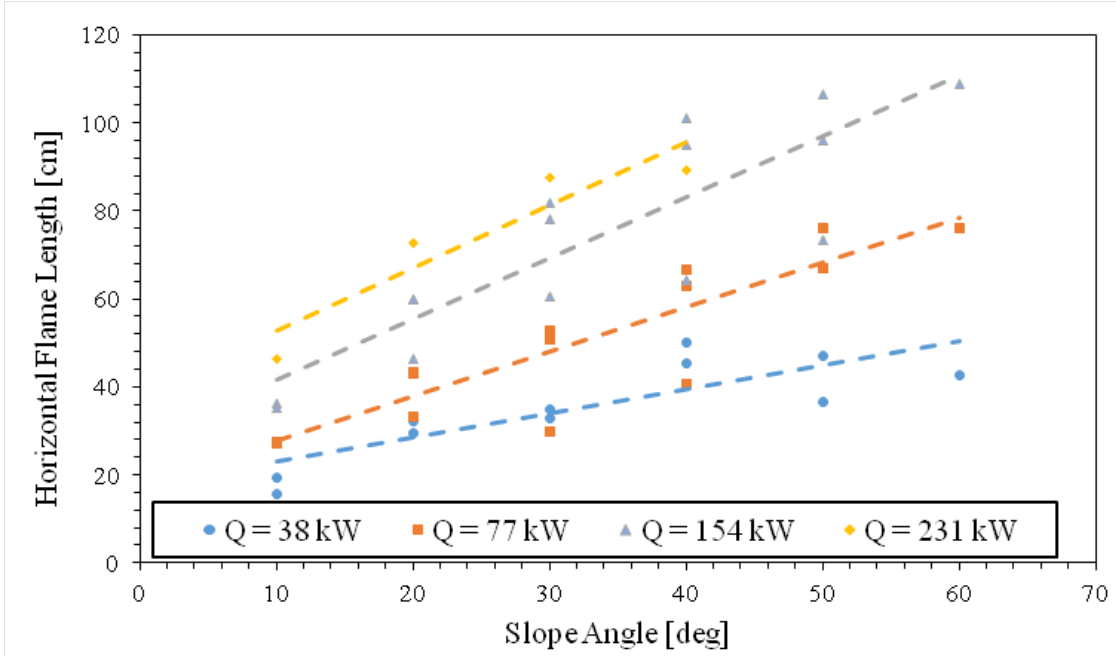
Figure 3.6: Horizontal flame height, x_f, versus the slope angle, θ, of large-scale inclined experiments for different fire sizes.
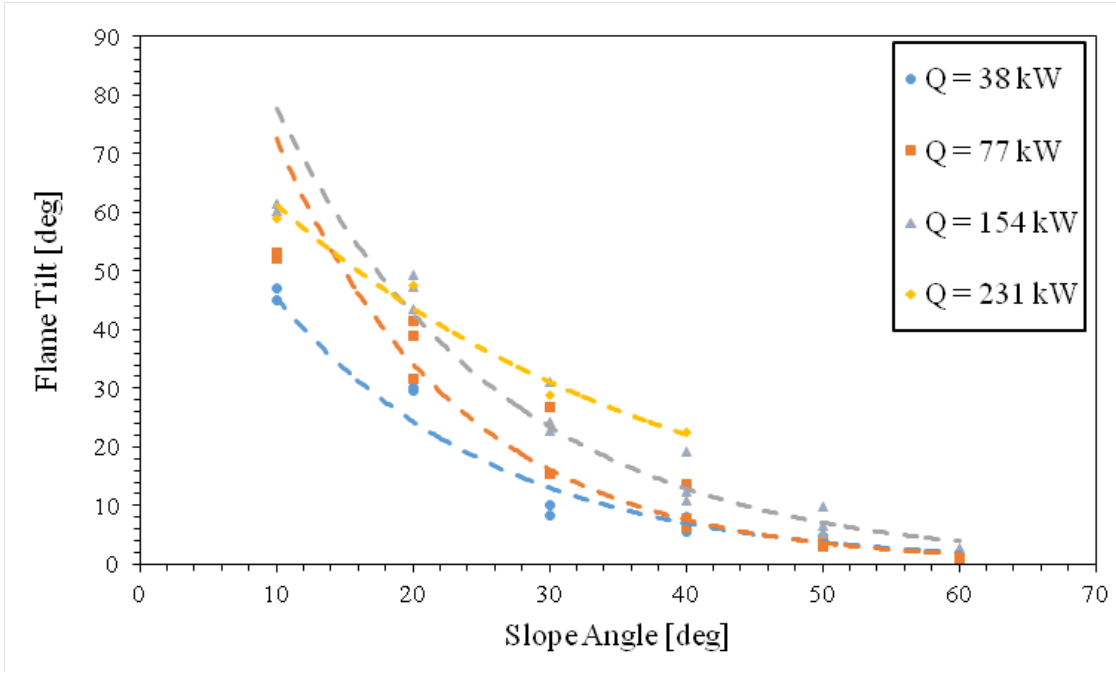
Figure 3.7: Flame tilt angle, ϕ, versus the slope angle, θ, of large-scale inclined experiments for different fire sizes.
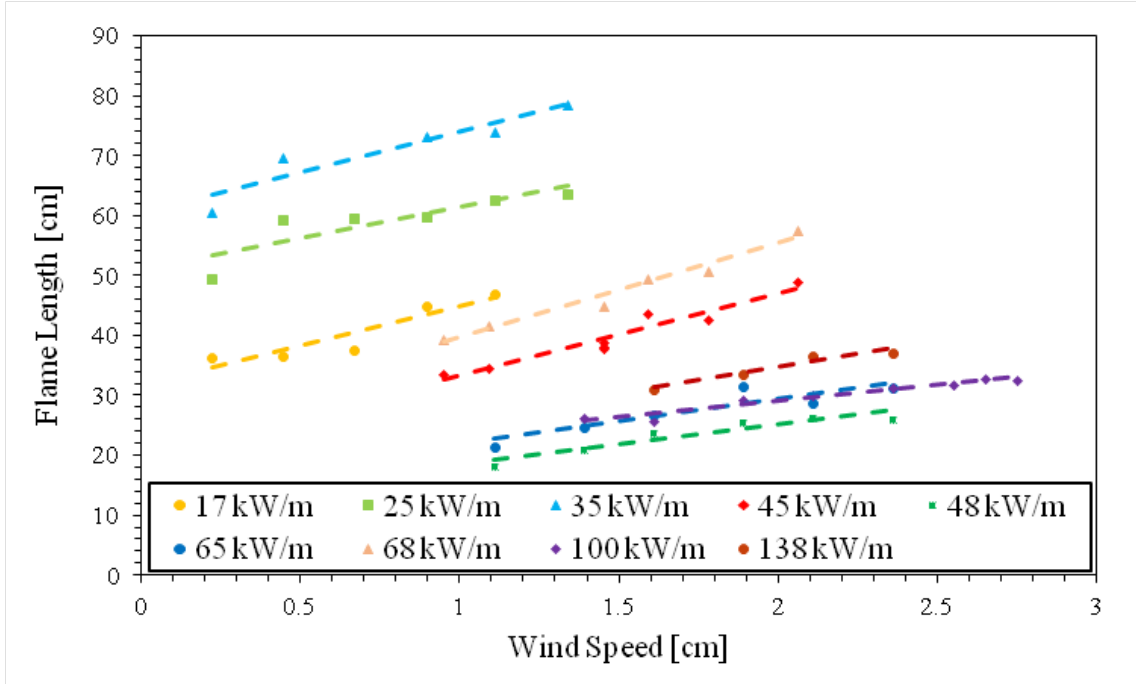
Figure 3.8: Flame length, L_f, versus wind speed, U.

and at UMD with the wind blower. The Missoula wind tunnel experiments used fire sizes of 17, 25, and 35 kW/m, and a burner depth of 24 cm. The experiments performed at UMD with the wind blower also appear to be segregated based on the burner used, with the heat-release rate per unit length of 45 and 68 kW/m were performed with the second iteration of the sand burner design, with a burner depth of 10 cm. The remaining data points, for fire sizes of 48, 65, 100, and 138 kW/m were performed with the initial sand burner with a depth of 4.54 cm.

Figure 3.8 shows how the centerline flame length, L_f, increases as the wind speed increases. There appears to be a grouping for the value of the flame length based on the burner depth. Experiments with the largest burner depth, 25 cm, are grouped relatively close for larger flame lengths.
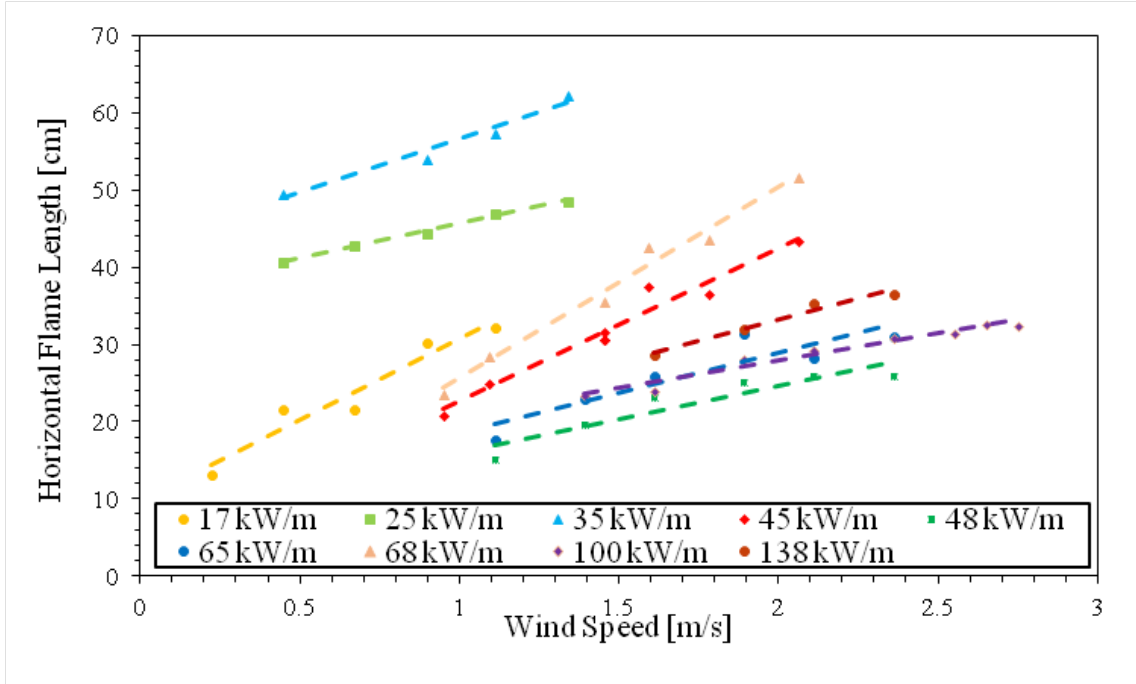
Figure 3.9: Horizontal flame length, x_f, versus wind speed, U.

Figure 3.9 shows the horizontal flame length, x_f, increases as the wind speed increases and Figure 3.10 shows the flame height, H_f versus the ambient wind speed. As the free-stream velocity increase, a nearly exponential decay in the flame height is observed. We would expect the flame height data to show a transition at some point from a plume-type fire to an attached (boundary-layer) flame, like in the inclined experiments, but there does not seem to be any distinguishable transition in this data.

Figure 3.11 shows how the flame tilt angle, ϕ decreases with increased wind speed. Similar to flame length measurements, the flame angle measurements are grouped based on the burner depth. There is a slight exponential relationship between the flame angle and the wind speed as an increased momentum flux from the
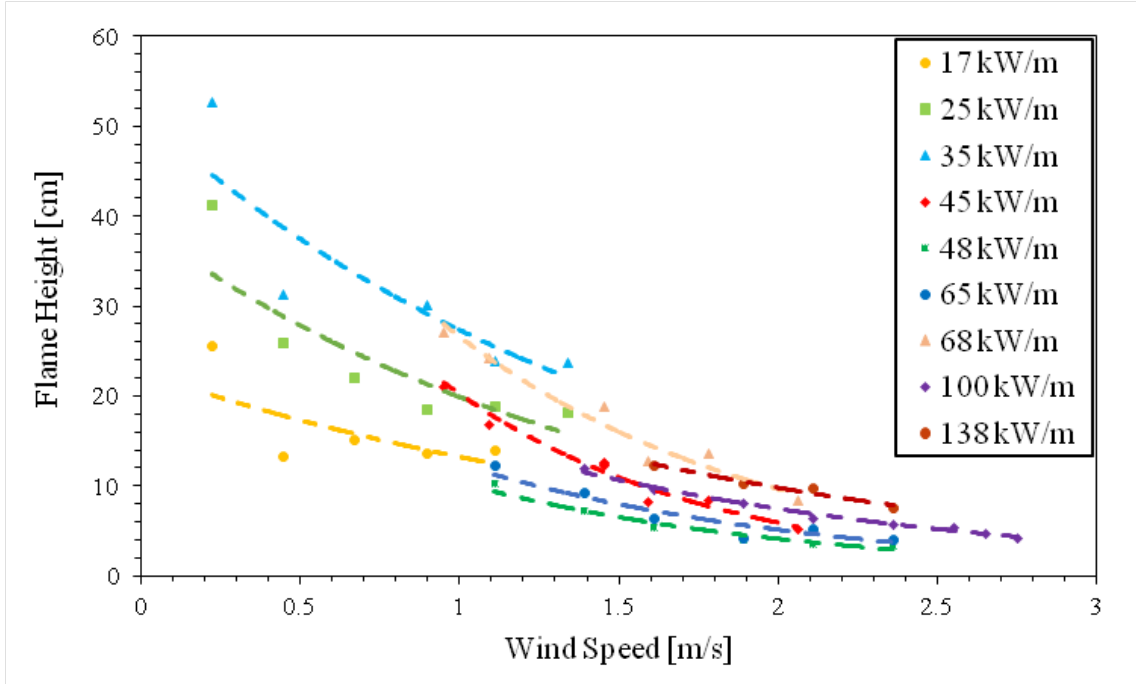
Figure 3.10: Flame height, H_f, versus wind speed, U.

incoming wind speed "pushes" the flame closer to attach to the surface.

3.2   Flame Pulsation and Intermittency

The downstream flame location in stationary experiments was determined using side-view high-speed video and an array of thermocouples ahead of the burner. A region starting at the downstream edge of the burner and extending fully downstream, 1 cm above the surface was determined as the region of interest where extension of the flame would relate to flame attachment and fuel particle heating. The flame extension downstream of the burning region is referred to as flame location or flame location, and denoted symbolically as x_e. This location fluctuated in
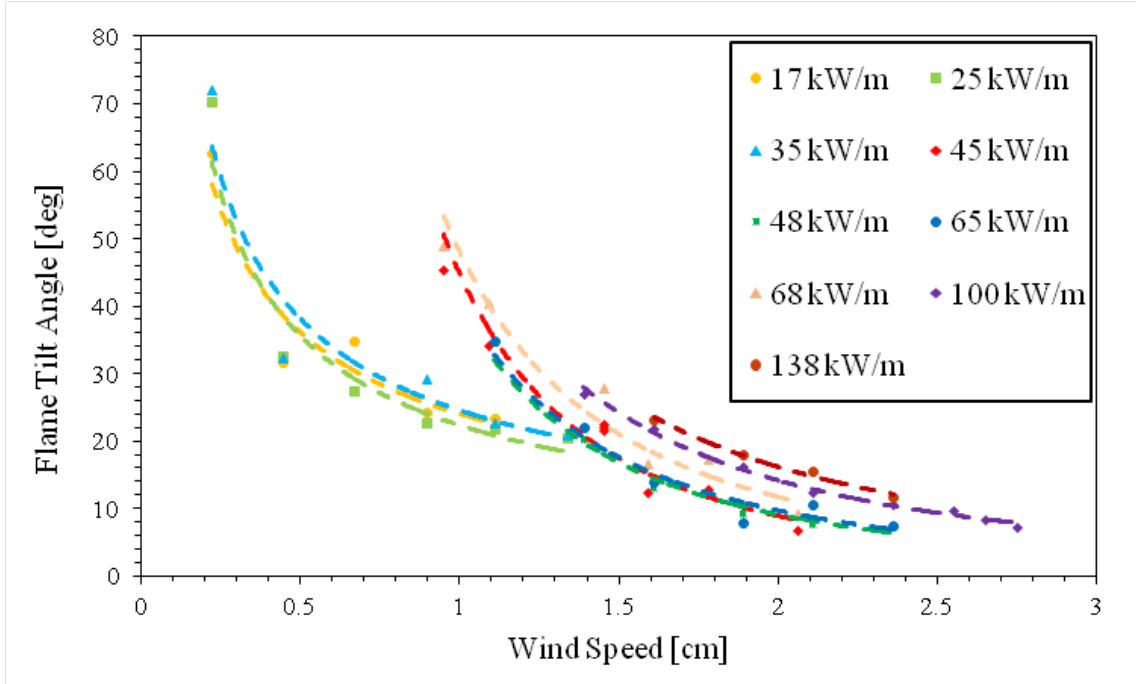
Figure 3.11: Flame tilt angle, ϕ, versus wind speed, U.

time as it was observed that the flame would pulse downstream, bursting into what would be the unburned fuel region in a spreading fire experiment.

Video analysis was performed using a MATLAB script and the *VideoReader* function to import the experimental video and decompose it into individual images. Flame distinction was made using the same threshold determined for mean flame geometry. Images were converted to black and white using this threshold level. The previously-described region-of-interest was defined from the downstream edge of the burner surface (user-input) to the end of the image in the downstream direction, with a height above the surface of 1 cm. Flame location, x_e, was then determined in this region-of-interest by tracking the furthest-most downstream tip of the flame. This location fluctuated in time, its downstream location shown for example in

41
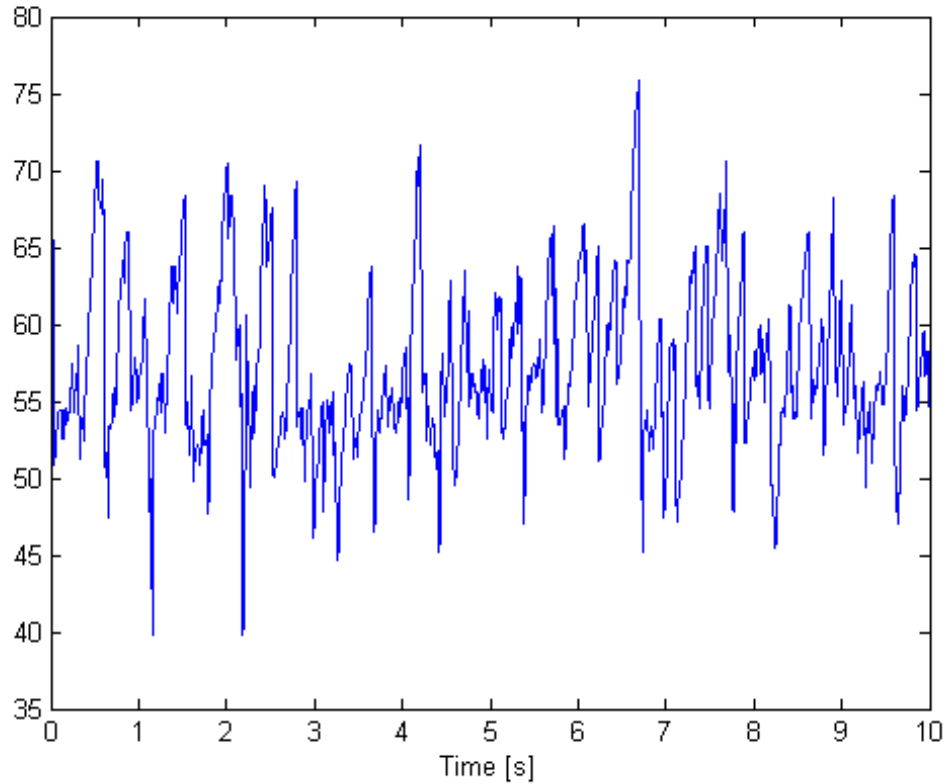
Figure 3.12: Sample flame location downstream of burner, x_e, versus time for large-scale inclined experiment. Heat-release rate = 154 kW, burner depth = 12.7 cm, slope angle = 30 deg.

Figure 3.12.

A method for determining a level-crossing rate was used on the flame location signal to determine the frequency of flame pulsations at points downstream of the burner. The crossing rate was determined for locations downstream of the burner in 1 cm increments and converted to a frequency based on the frame rate of the video. First, the index of all points in the flame location signal that were greater than the crossing location were determined. Then the indexes where the flame locations transition from below to above the crossing location were marked. A level-crossing

was only considered for one direction; therefore only when the flame was previously not at a location and then at the next time step it was counted a crossing. This is somewhat analogous to the variable-interval time averaging (VITA) technique use to study turbulent flow fluctuations, described elsewhere [27]. The crossing rate was then determined to be the number of flame location transitions divided by the number of frames in the video analyzed, and the frequency determined by multiplying the crossing rate by the frame rate of the video.

The frequency for different locations downstream were determined to look find the location of peak frequency (intermittency) (Figure 3.13). When a single frequency was needed for analysis, such as Strouhal-Froude scaling, the peak frequency was used.

The stochastic nature of the flame locations indicates there are a range of spectral-phenomena occurring. In order to compare the general variance a normal probability density function of the normalized flame location was determined. The flame location is normalized by dividing each individual flame location by the mean flame location. This was done to be able to compare the fluctuations in flame location for different fires sizes and slope/wind conditions. This density function captures how far the flame extends downstream beyond the mean flame location. Figure 3.14 shows and example where the wing of the PDF denotes the probability a flame will extend beyond the mean flame location.

A fast-fourier transform (FFT) from the time domain to the frequency domain can also be used to determine the critical frequency of the flame oscillations. Figure 3.15 shows a typical FFT plot of the flame location signal and it is clear that
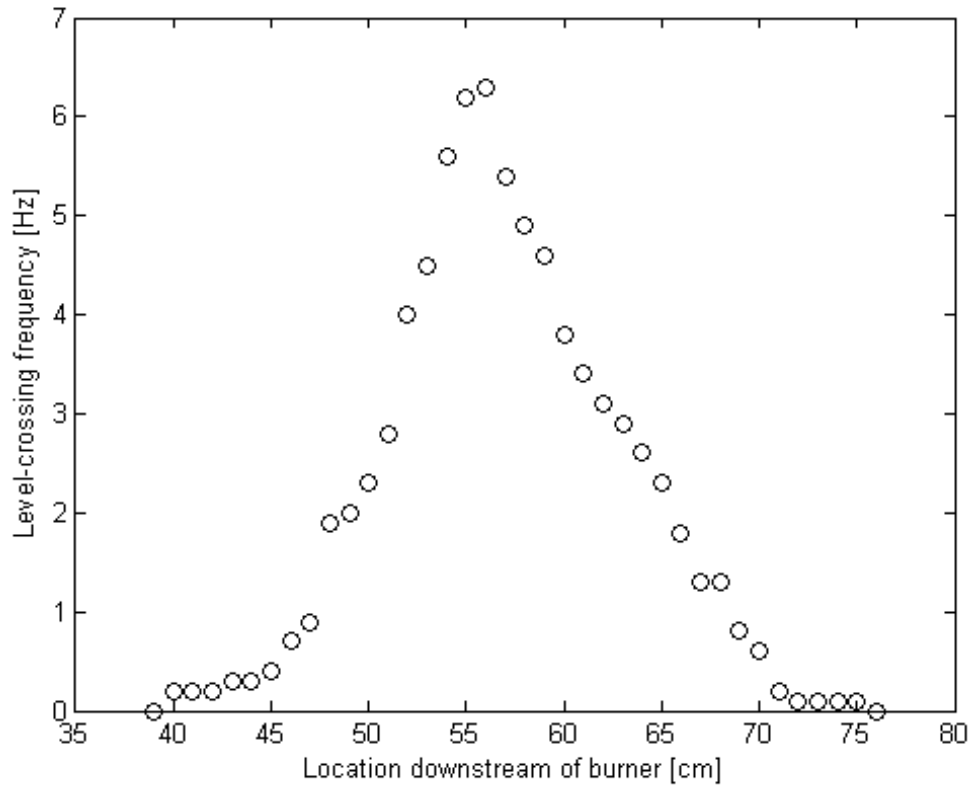
Figure 3.13: Sample level-crossing frequency at locations downstream of the burner for large-scale inclined experiment. Heat-release rate = 154 kW, burner depth = 12.7 cm, slope angle = 30 deg.
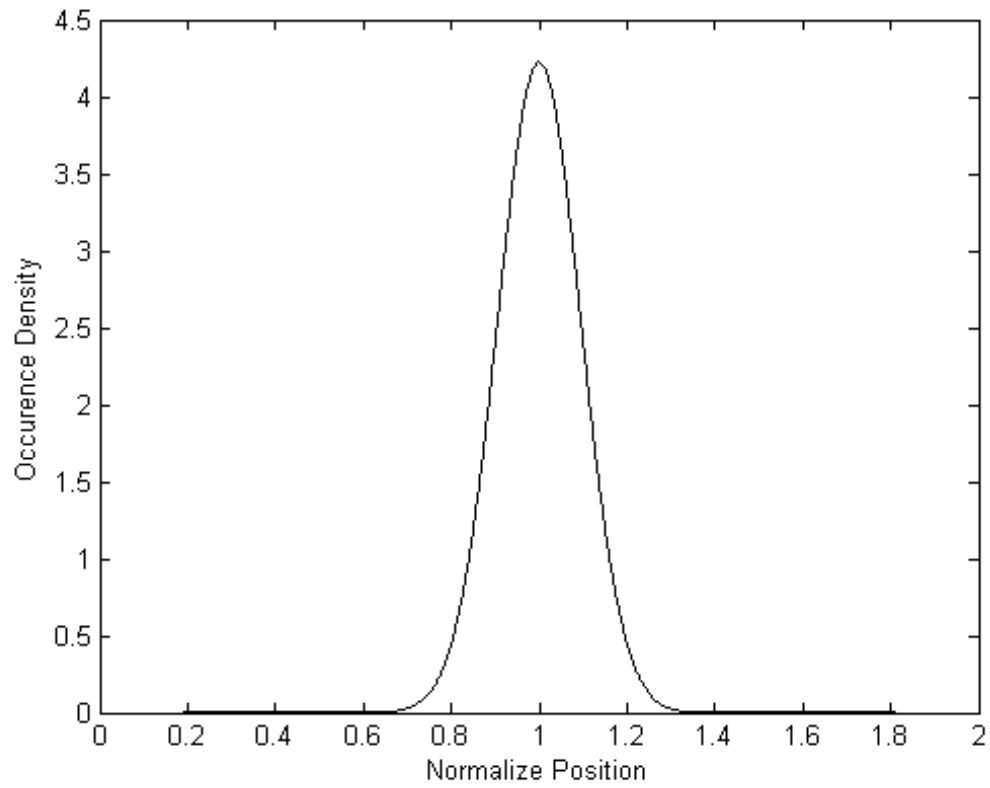
Figure 3.14: Sample probability-density function of normalized flame location for large-scale inclined experiment. Heat-release rate = 154 kW, burner depth = 12.7 cm, slope angle = 30 deg.
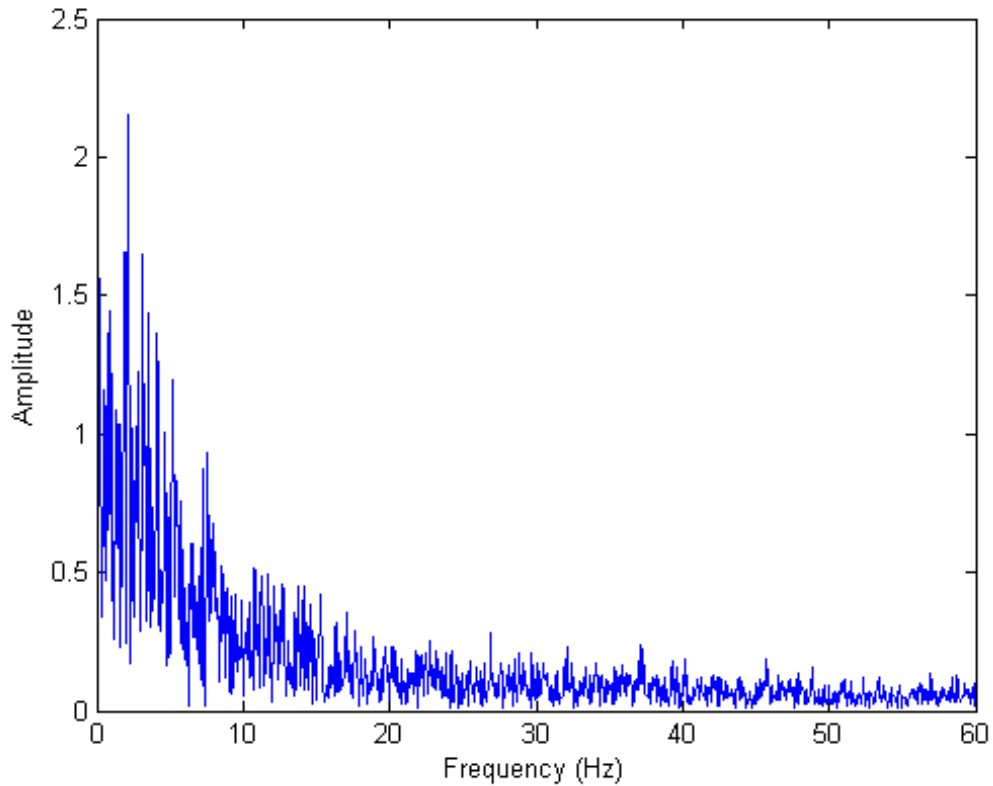
Figure 3.15: Sample fast-fourier transform of flame location signal for large-scale inclined experiment. Heat-release rate = 154 kW, burner depth = 12.7 cm, slope angle = 30 deg.

no dominant frequency is captured with this technique. No distinct but a range of frequencies appear in the signal. Similar to turbulent phenomena, stochastic process over a range of frequencies occur. This suggestions that that flame pulsation does not follow a sine-wave oscillation and more advanced spectral analyzes are required.

3.2.1 Inclined Experiments

Pulsation analysis results for large-scale inclined experiments are shown in Figures 3.16 - 3.19. Figure 3.16 shows how the peak level-crossing frequency increases
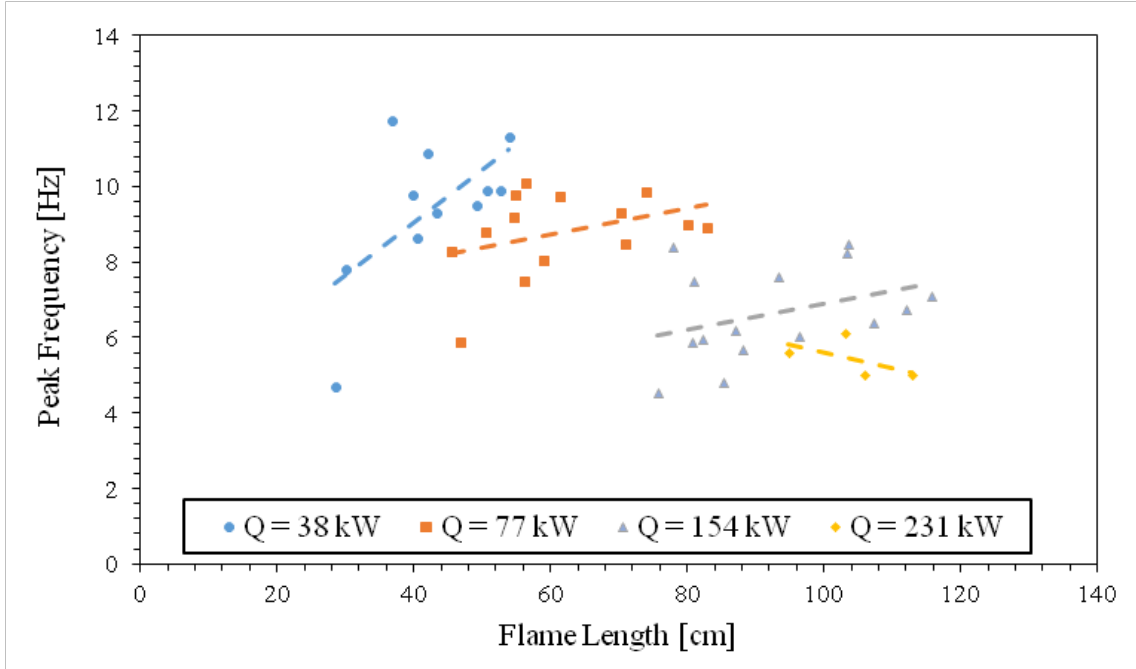
Figure 3.16: Pulsation frequency, f, versus flame length, L_f for large-scale inclined experiments.

slightly with the flame length and decreases slightly as the fire sizes decreases. A slight linear relationship between the peak frequency and the flame length for different heat-release rates suggests that the relationship between the frequency and flame length changes based on the fire size. The frequency is more sensitive for smaller fire sizes and less for larger fires, suggesting there is a dependence on plume or attached flame geometry.

Figure 3.19 shows the peak frequency plotted against the heat-release rate divided by the burner depth for different slope angles. Not much correlation is observed. The downstream distance with the observed peak frequency increases with both the flame length and fire size (Figure 3.18).
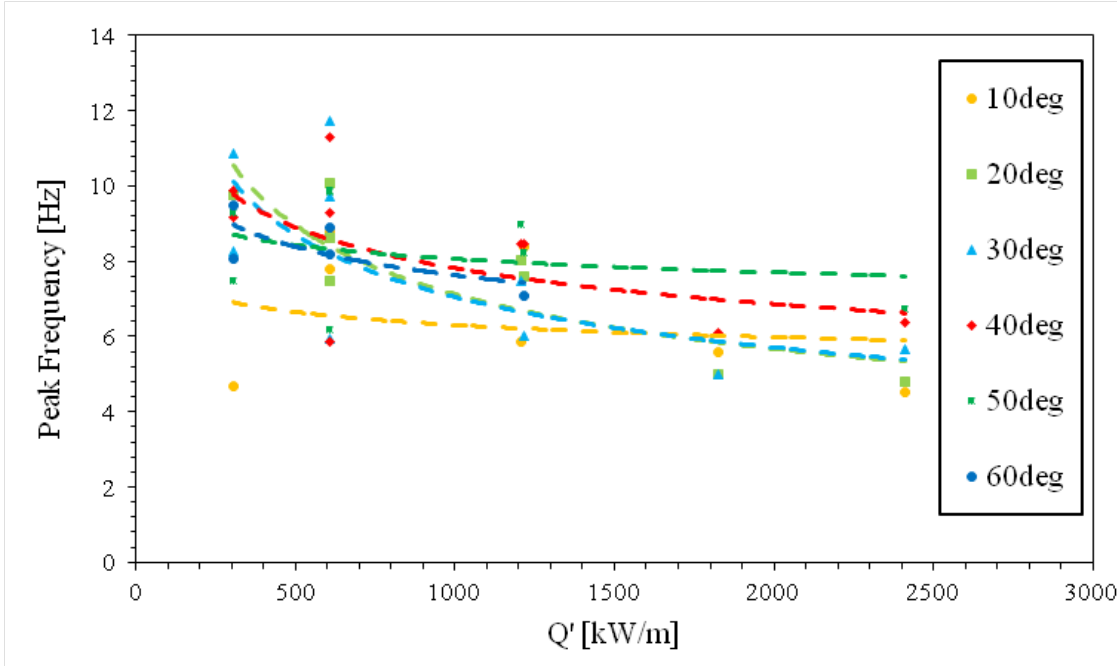
Figure 3.17: Pulsation frequency, f, versus heat-release per unit depth of burner, Q'.
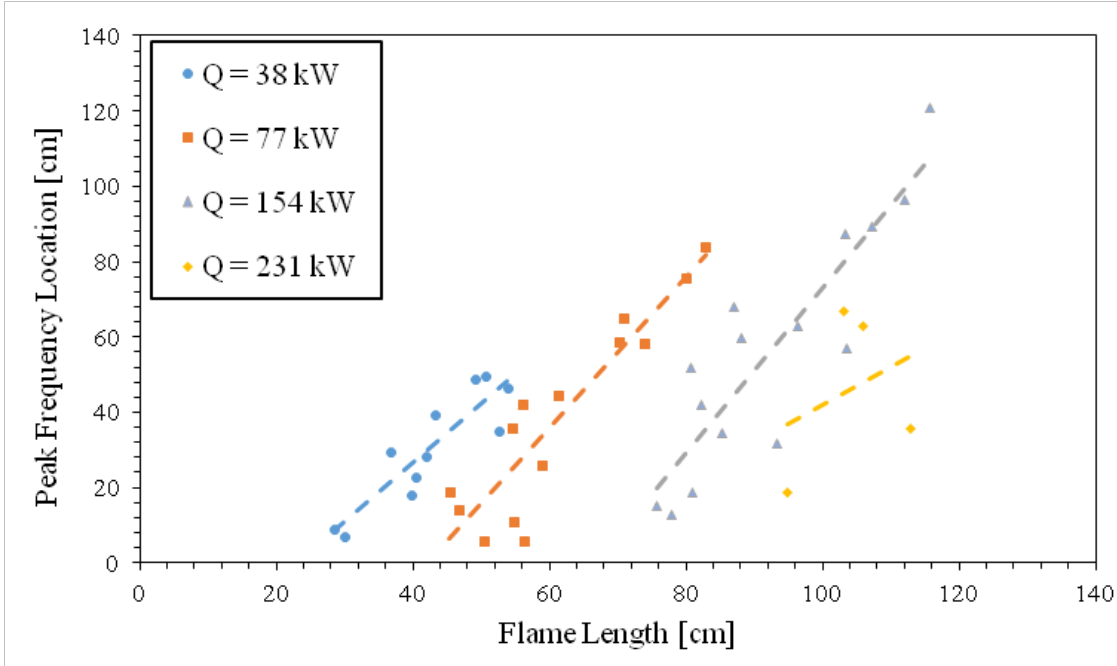
Figure 3.18: Peak frequency location versus flame length, L_f for large-scale inclined experiments.
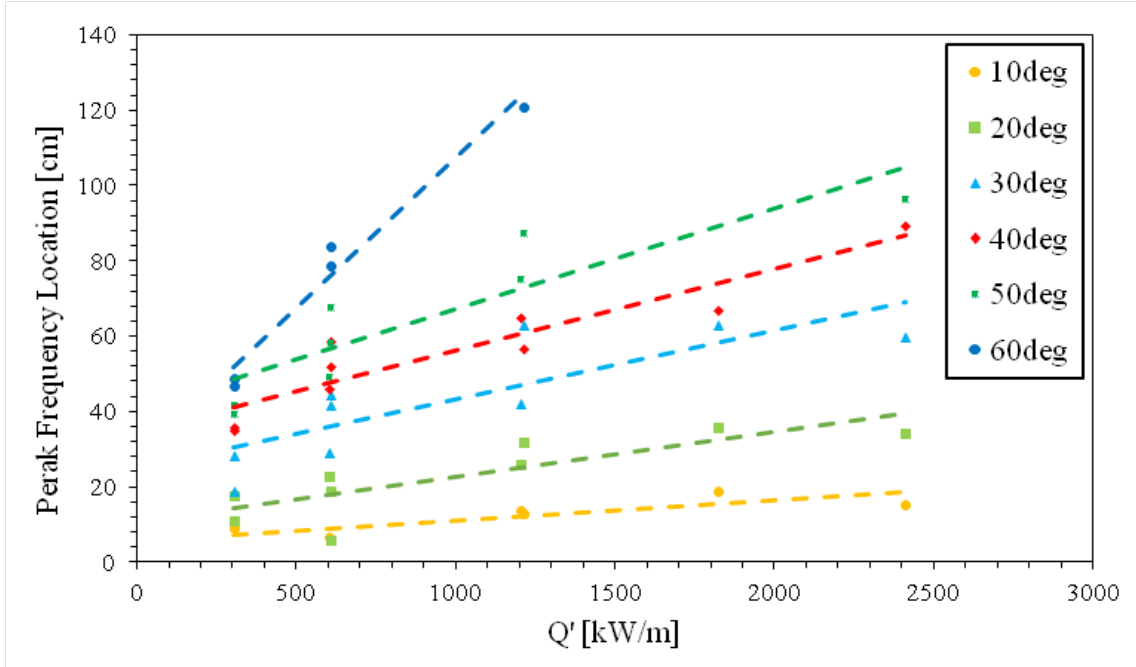
Figure 3.19: Peak frequency location versus heat-release per unit depth of burner, Q' for large-scale inclined experiments.

Figure 3.19 shows how the relationship between the peak frequency location and the heat-release divided by the burner depth increases in proportionality as the slope angle increases. This is similar to the relationship between the flame height and the slope angle at different fire sizes, the transition from a plume-fire to an attached fire occurs above 30 degrees, and this is where the peak frequency location increases more rapidly for larger fires.

3.2.2   Forced-flow Experiments

Pulsation analysis results for forced-flow experiments performed both in the Missoula wind tunnel and at UMD with the wind blower are shown below. Fig-
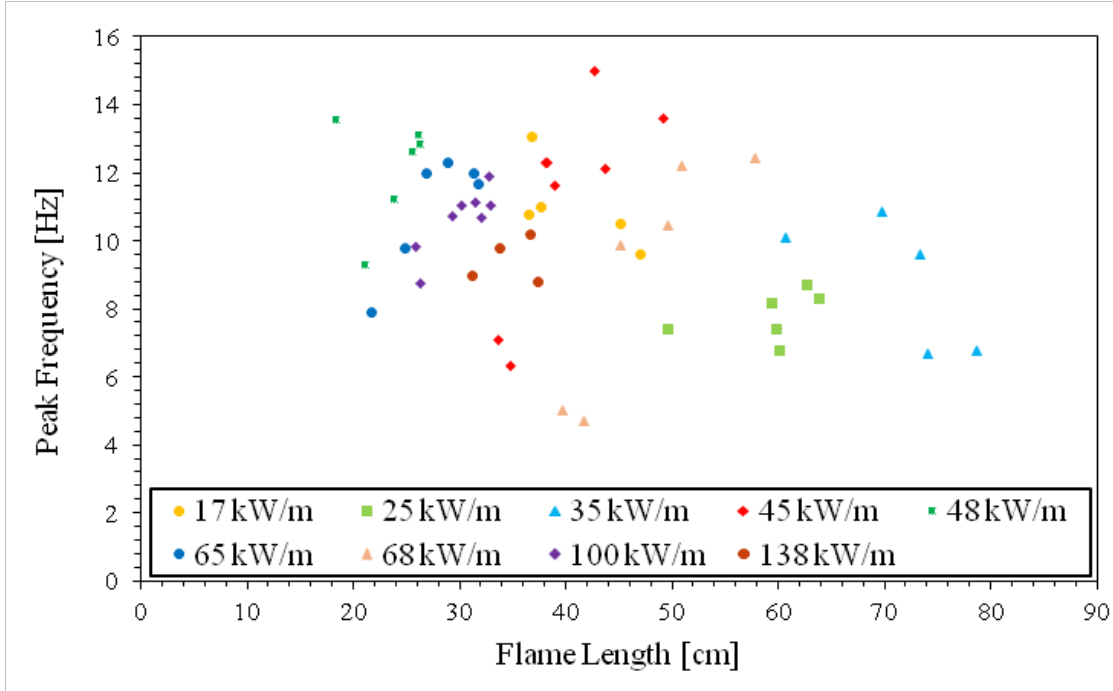
Figure 3.20: Peak pulsation frequency, f, versus flame length, L_f from forced-flow experiments.

ure 3.20 shows the peak frequency versus flame length for various heat-release rates divided by the depth of the burner. There is a slightly positive relationship between the flame length and peak frequency but no real trend with the heat-release per unit length.

The downstream distance of the peak frequency also increases as the flame length increase (Figure 3.21). For higher wind speeds the flame is tilted closer to the surface and the downstream reach of the flame increased. This means the flames are more likely to reach further into an burned fuel bed.

The relationship between the peak frequency location and flame length changes when the flame length is multiplied by the wind speed (Figure 3.22). The quantity
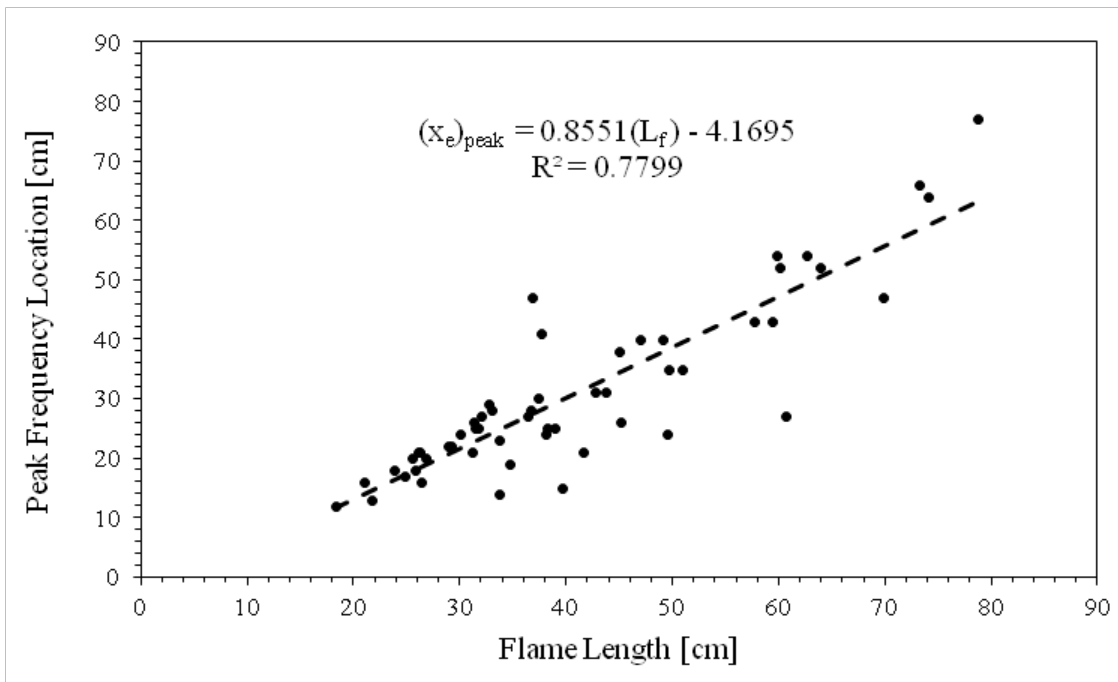
Figure 3.21: Peak frequency location versus flame length, L_f for forced-flow experiments.
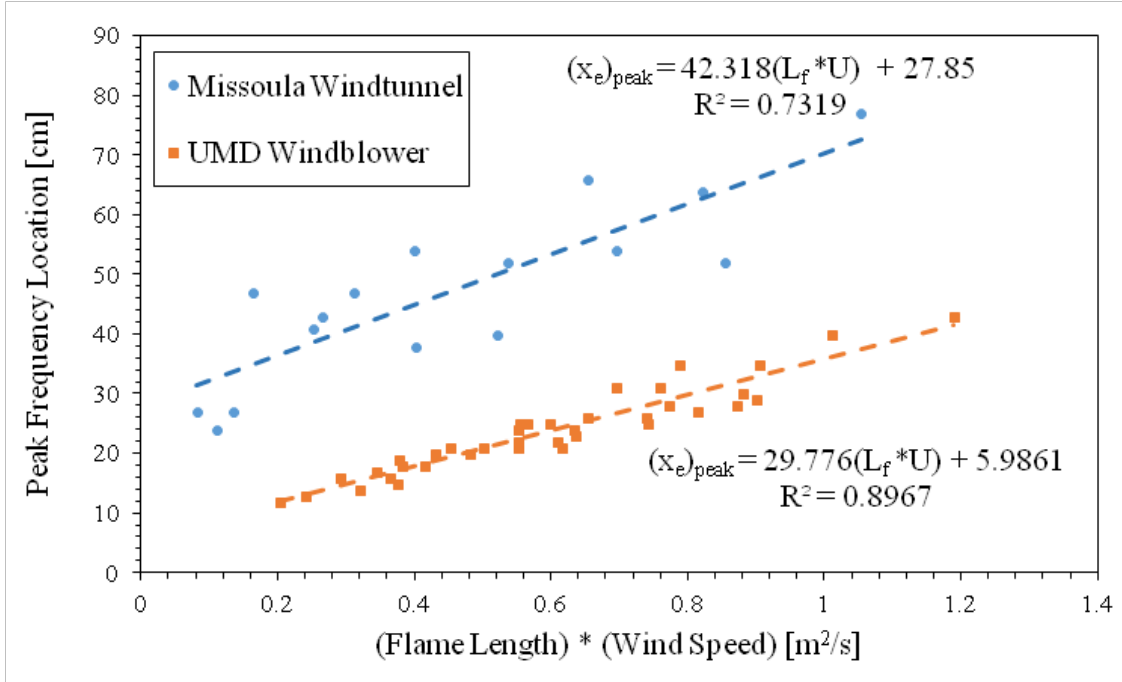
Figure 3.22: Peak pulsation frequency, f, versus the wind speed times flame length, UL_f.

of the flame length multiplied by the wind speed is a parameter that is attempting to capture effect of the wind pushing the flame closer to the downstream surface and the flame length which attaches to the surface. The relationship becomes more linear, but there is a clear distinction between experiments performed in the wind tunnel and ones performed with the wind blower (in Montana and Maryland, respectively). The incoming boundary-layer profile may cause this deviation between experiments, however the velocity profile above the burner in the Missoula wind tunnel is unknown.

3.3 Streamwise Streaks

Streaks in the flame were observed over stationary burners when wind was applied in the streamwise direction. These streaks are believed to be manifestations of peaks and troughs in the flame with associated increases or decreases luminosity caused by counter-rotating streamwise vortex pairs. These appear to be similar to previously described as Görtler vortices which occur over curved boundary-layers or on heated inclined plates [19]. The streak represents the upwash region at the intersection of two vortices, and so the space between the streaks contains a pair of streamwise vortices. The space between coherent streaks, λ, was determined using image analysis from the top view images of the experiments.

Image analysis was performed in MATLAB with the same readin process described for the flame pulsation analysis. The burner width was used in the images to set a scale for converting from pixels to length in centimeters. A crop box region was selected at the base of the flame where the streaks first formed across the width of the burner. The depth of the cropbox in the flow direction was set to 1 cm based on the scale set by the burner width. Each image was converted to gray-scale and cropped to the same area. The pixel value in each column of the cropbox was averaged and a light intensity signal across the width of the burner was produced. Figure 3.23 is a sample of the light intensity across the width of the burner. The local peak in the signal is determined and marked as black triangles on the plot. These points represent streaks in the flame, otherwise seen as flame peaks in the streamwise flow.
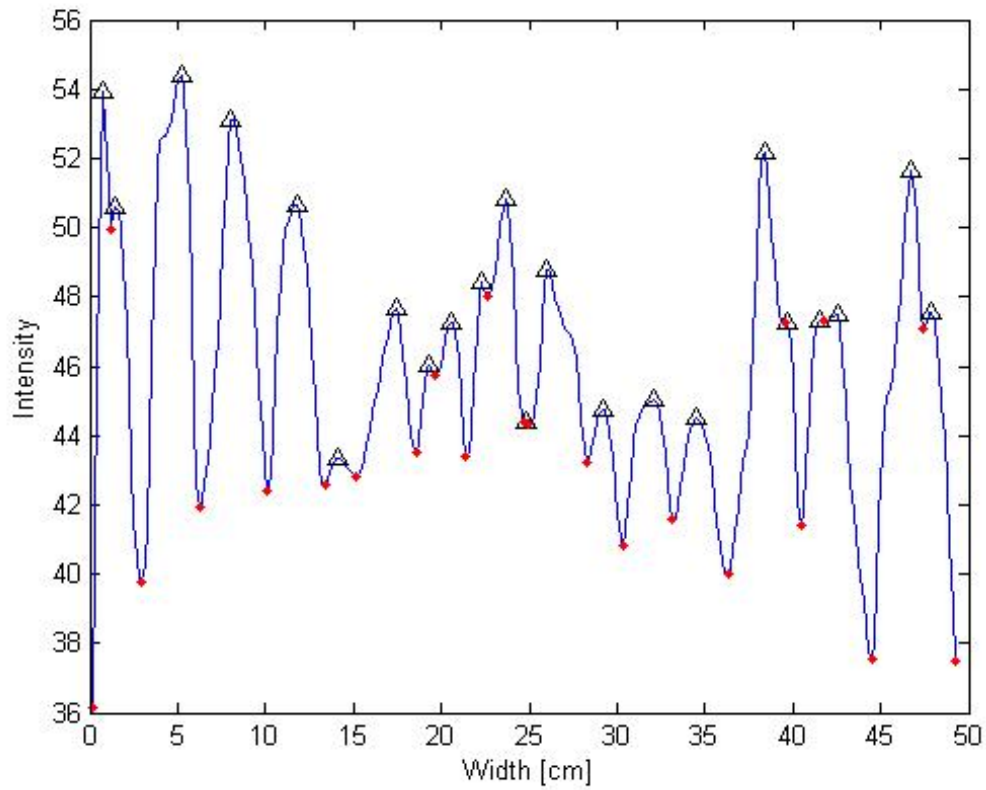
Figure 3.23: Light intensity across the width of the burning region for a single image. The local maximums in the light intensity are marked with black triangles and represent flame peaks.

The average spacing for each image was determined and all images in an experimental set analyzed. The streak spacing distribution was plotted as a histogram to show the distribution over the length of the experiment (Figure 3.24). The streak spacings were found to follow a log-normal distribution and so a probability density function was fit with the data. This follows analysis for streak-like structures found in other turbulent boundary-layer flows [28], where despite sinuous meandering of the streaks they maintain constant mean spacings. The streak spacing for an experiment was taken from the peak of the log-normal function from the streak spacing distribution.

3.3.1 Inclined Experiments

The streak spacing for all inclined experiments versus the flame length is shown in Figure 3.25. The streak spacing does not change much with the flame length, but decreases slightly as the flame length increases. The arithmetic mean of the streak spacing for all experiments is $\lambda_{mean} = 1.88$ cm with a standard deviation of $\sigma = 0.16$. This is a variance of less than 8% for the range of experiments; it appears that the controlling parameter in the streamwise vortice formation and spacing was not captured in these experiments, however they were able to be more reliably produced and statistically analyzed then for spreading experiments
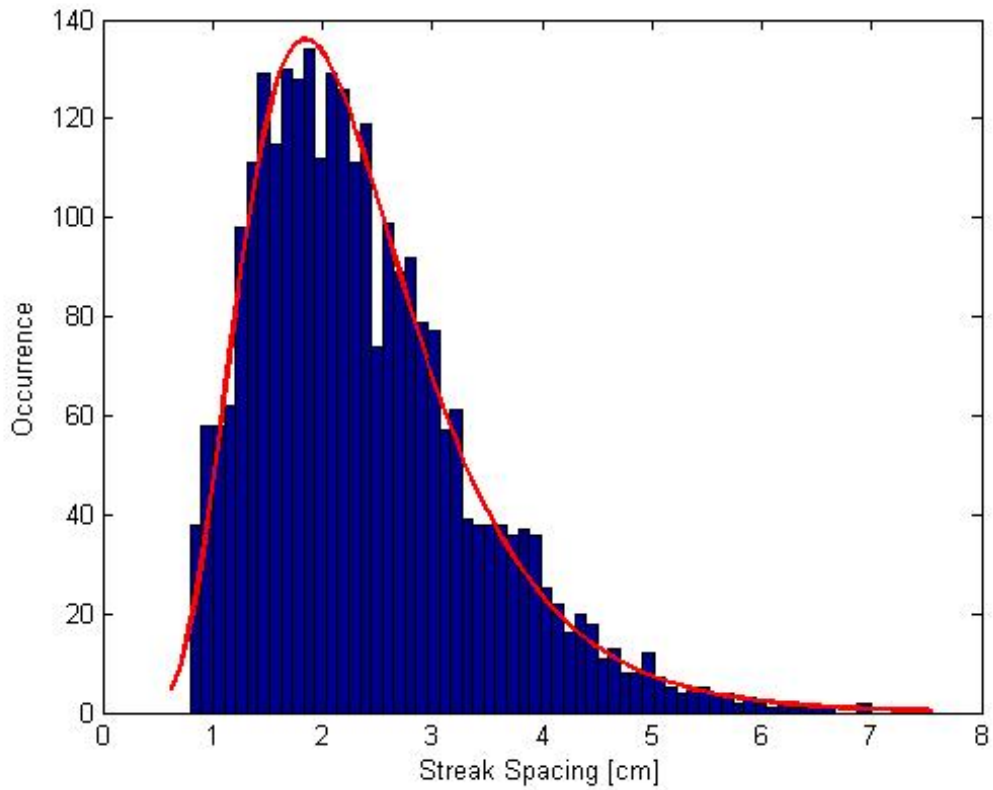
Figure 3.24: Histogram of streak spacing over the length of an experiment. A log-normal probability density function distribution was fit to the data and is shown with the bold red line.
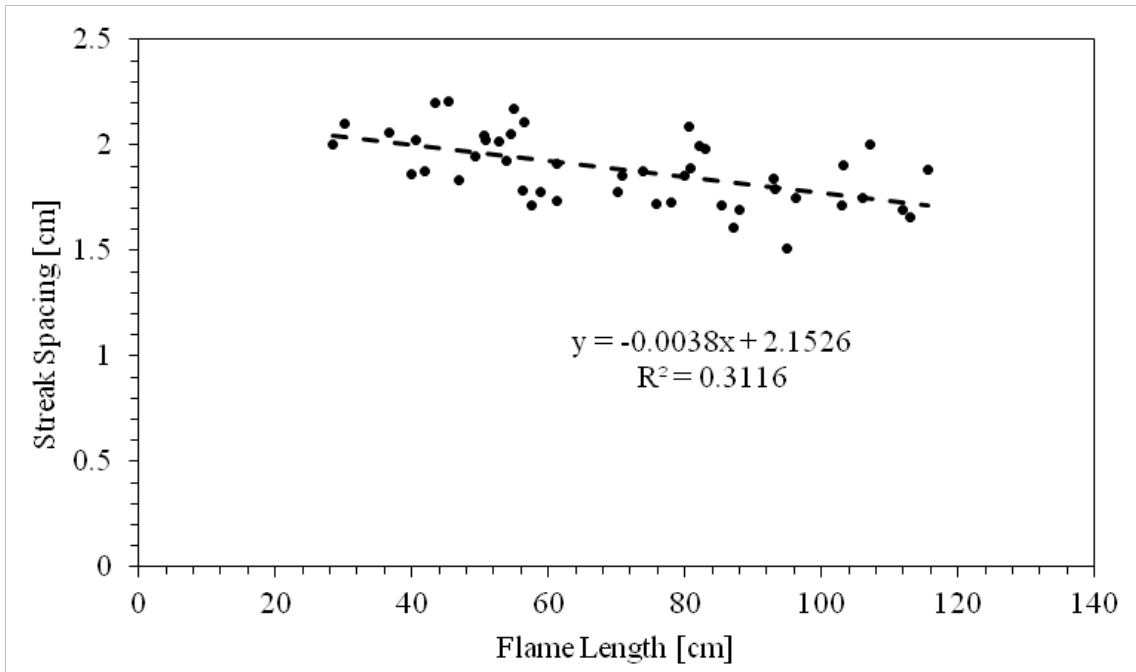
Figure 3.25: Streamwise streak spacing, λ, versus flame length, L_f from large-scale inclined experiments.
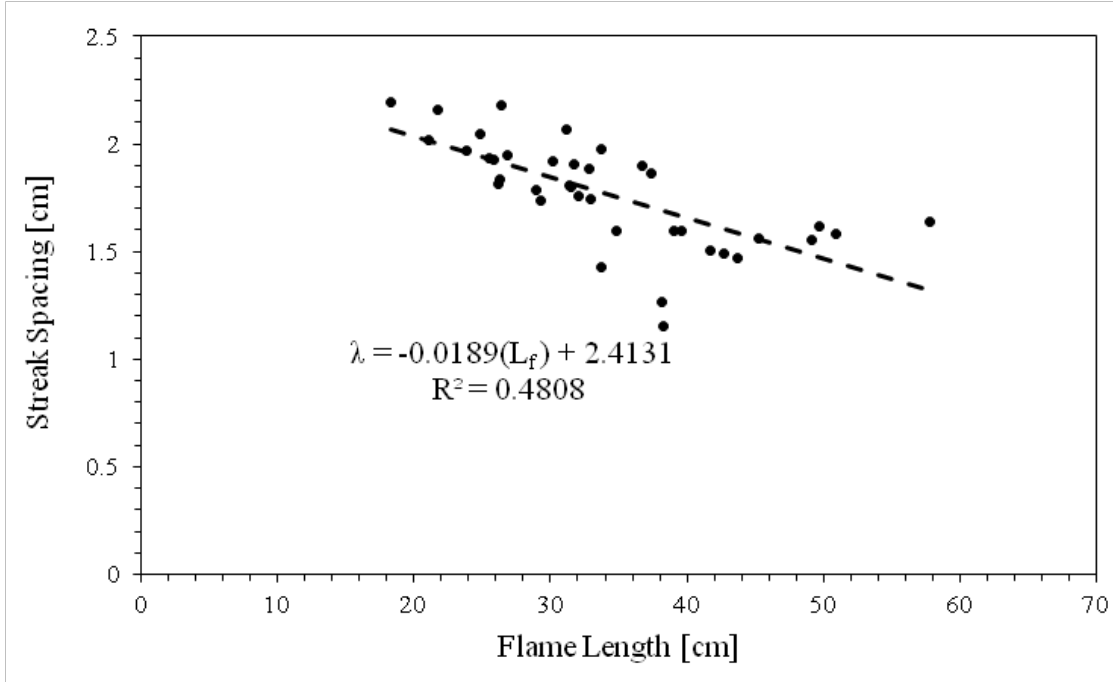
Figure 3.26: Streamwise streak spacing, λ, versus the flame length, L_f from forced-flow experiments.

3.3.2 Forced-flow

Streak spacing for forced flow experiments were compared with the flame length in Figure 3.26. A slight decrease in the spacing was observed as the flame length increases but the change in was very slight, the average streak spacing for all experiments is $\lambda_{mean} = 1.77$ cm with a standard deviation of $\sigma = 0.24$. Like the inclined results for streak spacing, the variance in streak spacing over the range of experiments performed here is very low.

3.4 Thermocouple Data

Thermocouple data was collected for some of the large-scale inclined experiments. Many of the thermocouples broke during the experiments because of the high temperature of the ethylene flame. The metal holder used to hold the thermocouples 1 cm above the surface warped from the constant heating of the flame. This caused the thermocouples to break or move significantly out of the region of interest. Due to unreliable data recorded, comparisons with video data are not presented here.

Chapter 4: Discussion

4.1 Strouhal-Froude Flame Pulsation Relationship

Figure 4.1 a Strouhal-Froude relationship, which is based on forced-flow experiments. The Strouhal and Froude number were previously defined in equations 1.4 and 1.1, and the relationship between the two is

$$\text{St} = 2\text{Fr}^{-0.5}. \tag{4.1}$$

The value of the exponent is slightly above the value of -0.43 found in scaling for larger-scale wind-driven spreading fire experiments [29] and the same for diameter scaling of puffing in circular pool fires [30]. While the flame length may not be the most fundamental quantity for scaling analysis because of its coupling to experimental conditions, it is useful as most wildland fire spread analyses are correlated to this quantity [31].

The agreement in this scaling between stationary and spreading fire experiments suggests that the methods of the experiments performed here can be used to study the same phenomena in spreading fires. The Strouhal number captures the pulsation of the flame close to the fuels causing intermittent contact, and the Froude
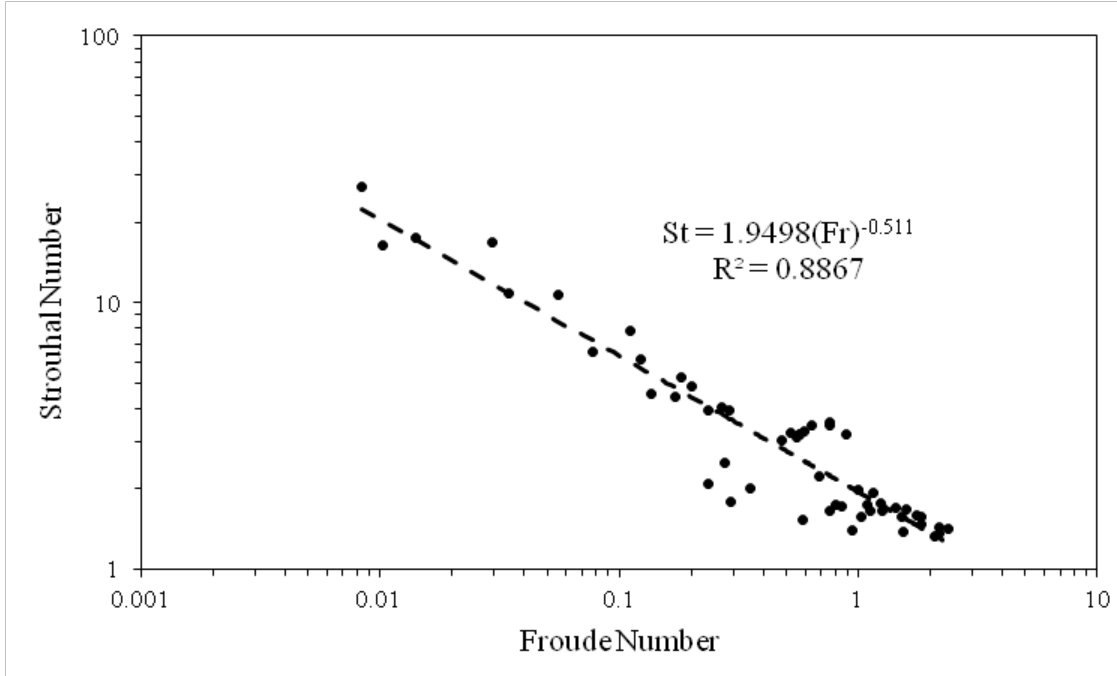
Figure 4.1: Strouhal-Froude scaling for stationary burner experiments performed with the wind tunnel and wind blower.

number represents the balance of forces from the wind and buoyancy of the flame. It could be possible to use this scaling to develop a relationship between the pulsing frequency for a range of wind conditions and fire sizes. A spread rate could possibly be determined based on the frequency and distance ahead of the flame front. In future studies, less reliance on the flame length as a length scale is desired, however it still provides a useful and practical representation of the fire size to scale buoyant effects.

4.2 Dimensionless Fire Length and Fire Size

A dimensionless length scale is often used in the fire research community to describe the buoyant source strength of fire [32]. D^*,

$$D^* = \left[\frac{Q}{\rho c_p T g} \right]^{2/5} \tag{4.2}$$

is given by the ratio of the fire heat release-rate Q to the ambient air conditions $\rho c_p T$ (density, specific heat, and temperature) and the square root of g, the acceleration due to gravity, all raised to the 2/5 power (Eq 4.2). The gravity term contributes to the buoyant force of the fire, and should act parallel to the line of action of the flame. To incorporate the slope angle of inclined fires, a rotated gravity vector term parallel to the inclined surface is used, given by the acceleration due to gravity time the sine of the slope angle:

$$g_{inclined} = g \sin(\theta). \tag{4.3}$$

Flame lengths of pool fires, for instance, can be scaled with the dimensionless fire length, and so with an adjusted gravity vector (Eq 4.3 they should be able to as well.

$$D^* = \left[\frac{Q}{\rho c_p T g_{incline}} \right]^{2/5} \tag{4.4}$$

The dimensionless fire length using the inclined gravity component (Eq 4.4) can be used to correlate the flame length of the large-scale inclined fire experiments

(Figure 4.2). The flame length increases linearly with D^* by a factor of 1.2 and based on the definition of this parameter it suggests that the flame length is dependent on the source fire conditions and slope angle. An attempt was made to capture the burner depth parameter in the flame length relationship as well, but unfortunately using a D^* equation with the heat-release divided by the burner depth did not correlate well.
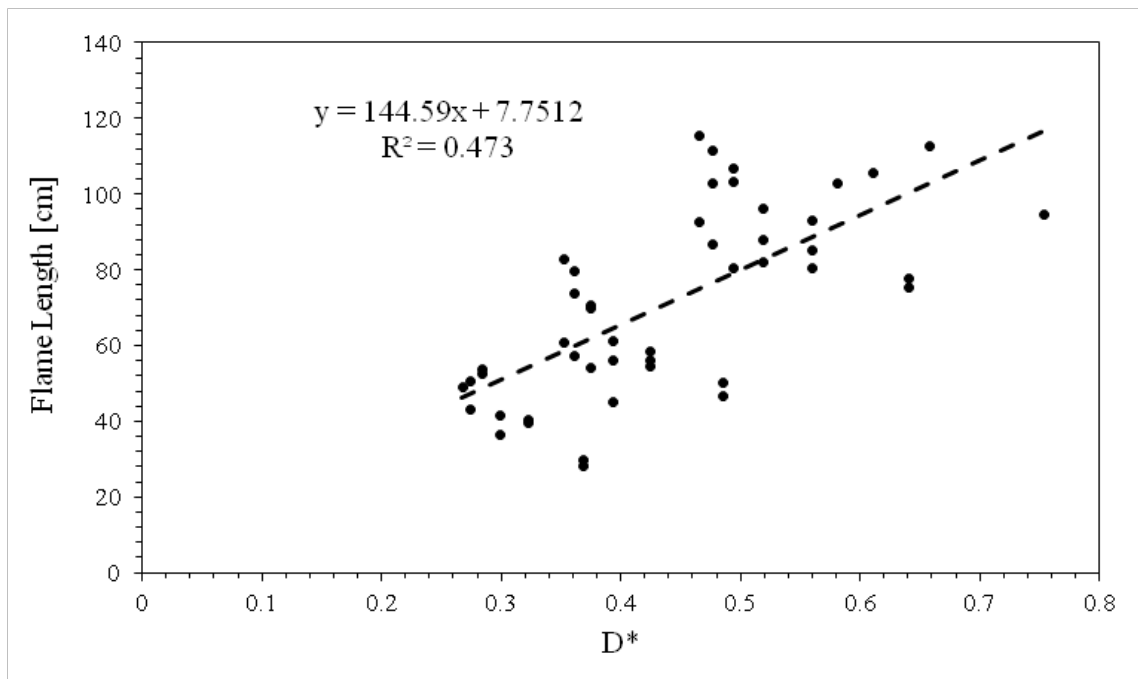
Figure 4.2: Flame length, L_f, versus dimensionless fire length, D^* for large-scale inclined fires.

Another common fire scaling parameter is the dimensionless fire size, Q^*, given by the dimensionless fire length D^* and a physical length scale, both raised to the 5/2 power. Often times the characteristic length scale is a plume dimension, so here we use the flame length, L_f (Eq 4.5),
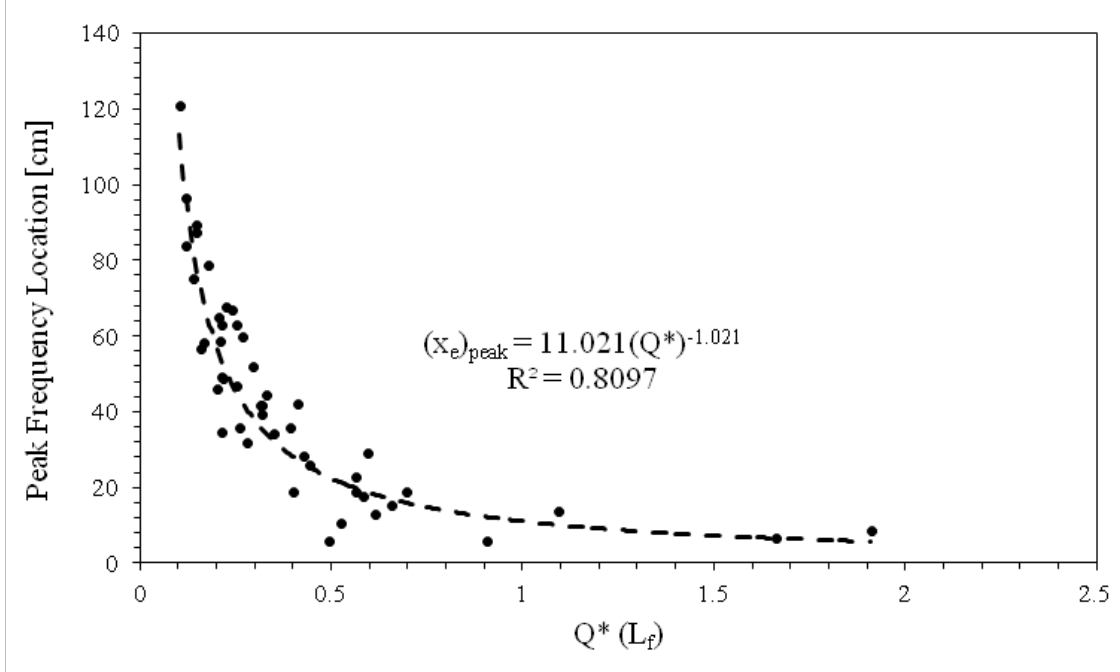
Figure 4.3: Location of peak frequency versus dimensionless fire size, Q^* for large-scale inclined experiments.

$$Q^* = \frac{(D^*)^{5/2}}{(L_f)^{5/2}}. \tag{4.5}$$

Figure 4.3 shows the location of the peak level-crossing frequency versus this dimensionless fire size parameter. The relationship shows the pulsation distance decreasing as the dimensionless fire size increases.

4.3 Flame Location Probability Density

The density function of the normalized flame location shows when the flame extended or "pulsed" further downstream than the average flame location. The far regions of the function can be considered "rare events" when the flame pulses much
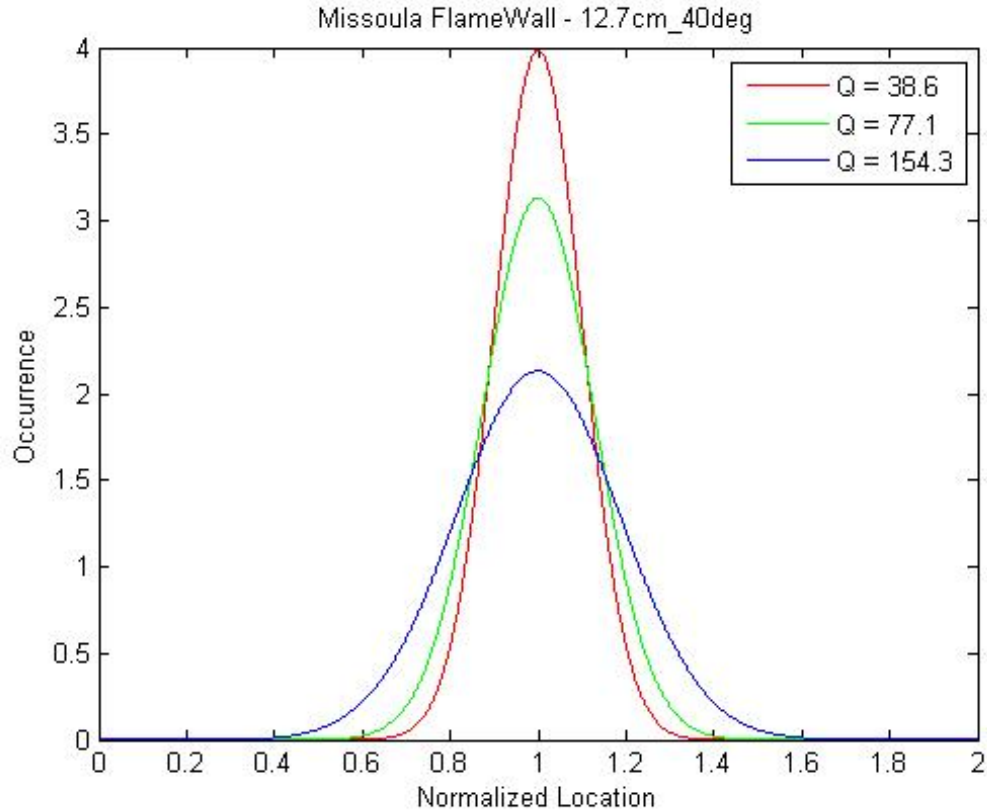
Figure 4.4: Probability density function of normalized flame location for three large-scale inclined experiments at 40 degrees with a burner depth of 12.7 cm and fire sizes of 38, 77, and 154 kW.

further downstream of the burning region, into unburned fuels. The probability of these rare events increase for the same wind or slope conditions but for increase fire size (heat-release rate, Q), as shown in Figure 4.4. Correlations of increasing flame extension frequency with slope angle, wind speed, and others parameters were poor compared to the strong correlation of fire size and increased extension frequency. This is perhaps because larger coherent structures develop in more intense turbulent fires, which can similarly cause increased flame spread rates.

4.4 Görtler Number Streak Formation

The Görtler number

$$G = \frac{U\theta_m}{\nu}\left(\frac{\theta_m}{R}\right)^{1/2} \tag{4.6}$$

is a dimensionless numbered that is used to determine the when Gortler vortices will form in boundary layers over curved surfaces [19]. This dimensionless number was developed to describe streak formation over a concave surface where θ_m is the momentum thickness of the incoming boundary layer and R is the radius of curvature of the wall. Görtler instabilities have been shown to develop at G greater that 0.3. The centripetal force is critical in the formation and so is captured by the radius of curvature. For the experiments performed in this thesis the buoyant force may be thought of as the centripetal force and so the radius is replaced by the flame length for the length scale,

$$G = \frac{U\theta_m}{\nu}\left(\frac{\theta_m}{L_f}\right)^{1/2}. \tag{4.7}$$

Figure 4.5 shows the Görtler number for forced-flow experiments conducted with the wind blower at UMD, where the momentum thickness was determined using a hot-wire anemometer. All values in this velocity range exceed the predicted onset value which is given for the original formation of the Görtler number with centripetal force.

Figure 4.6 shows the streak spacing as a function of the Görtler number and
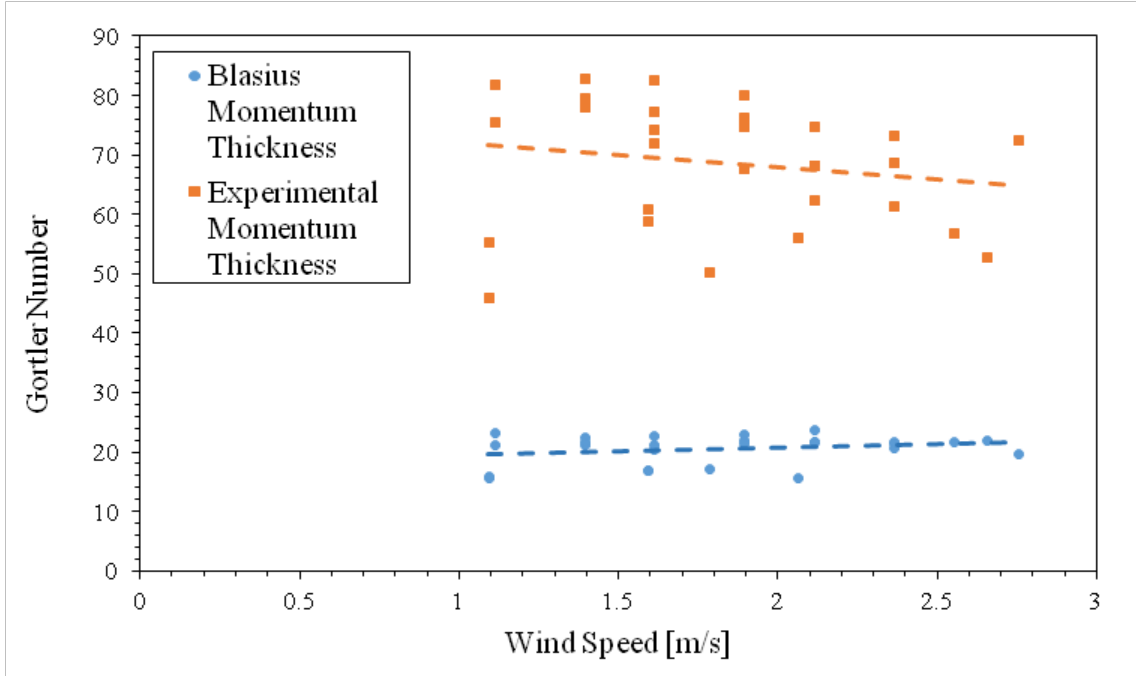
Figure 4.5: Görtler number plotted versus the wind speed for two different methods of determining the momentum thickness θ_m. The Blasius momentum thickness comes from the Blasius solution for boundary-layer flow over a flat plate. The experimental momentum thickness comes from velocity profiles measured with the hot-wire anemometer.

shows a good relationship for correlations of the streak spacing (given the limited range of values). A relationship between the flame length and large-scale streaks has been shown for spreading experiments, but an understanding based on the boundary-layer conditions is needed for these vortex structures.

4.5   Boundary Layer Effects on Streak Formation

One of the benefits of the small-scale forced-flow experiments at UMD was the use of a fully characterized wind blower. The wind blower was calibrated with a hot-wire anemometer as described previously. Using the hot-wire it was determined that
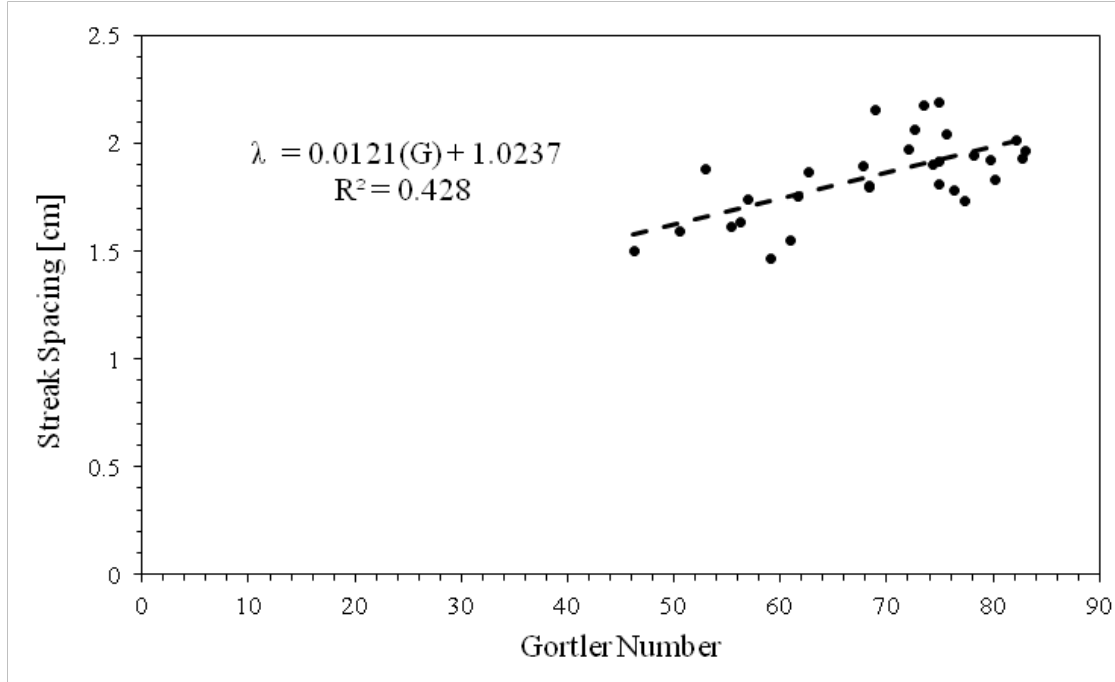
Figure 4.6: Streak spacing, versus the Görtler number calculated with the experimentally-measured momentum thickness.

the turbulence intensity of the flow was less than 3% at all points in the flow. With these calibrations the properties of the hydrodynamic boundary layer are known and can be used to understanding observations of streaks in the flame.

The incoming boundary layer across the burner was changed by the length of the flat boundary layer development surface upstream of the burner. For a short boundary layer development length, the top surface of the apparatus was raised approximately 2.54 cm above the bottom surface of the blower exhaust duct. This raised the insulation board out of the boundary layer that developed in the duct. A long boundary layer development length was achieved by making the top of the insulation board flush with the outlet of the blower exhaust duct and making the

connect seamless with aluminum tape.

Figure 4.7 shows the effects of the boundary layer development length on the formation of streamwise streaks above the burner surface. These pictures are from experiments with a heptane fuel soaked wicks with the same initial amount of fuel (120 mL). The difference between these two experiments is the boundary layer development length, x_{BLD}, which is the length of flat surface upsteam of the burner. The difference between the two cases is visually obvious; with no boundary layer development length the uniform flow generated flame with no boundary layer development has almost no observable streaks, with a flatter, more laminar appearance while the case with a boundary layer development length forms coherent streaks. Analysis of the two configurations showed that the boundary-layer configuration results in higher burning rates (0.8 g/s vs. 0.3 g/s), and higher peak frequencies than the uniform-flow configuration (7.3 Hz vs. 3.5 Hz). Therefore, the formation of streaks appears to be important in understanding downstream heating and thus fire spread.

Streak merging downstream of the burner formed into flame towers can be observed in top-view images. A successful method for tracking the merging of the streaks downstream was not determined, but based on visual observations the streamwise streaks clearly converge to form the flame towers. This may be associated with spanwise fluctuations of streaks at the base of the flame.

Figure 4.7: The incoming boundary layer has an obvious effects on the formation of streamwise streaks and properties of the flame. These two pictures are from experiments using 30 × 12 cm wick, soaked with 120 mL of heptane fuel, in 1.3 m/s forced-flow. In the picture on the left the leading edge of the burner is parallel with the blower outlet, and on the right there is a 28 cm inert surface upstream of the wick.

Chapter 5:   Conclusion

This study has presented a framework for the use of stationary gas burners to study spreading wildland fire behavior, enabling measurements and analysis of key parameters related to mean flame geometry and temporal fluctuations that play a role in flame spread. Video and micro-thermocouple techniques used to accomplish this are shown, as well as preliminary scaling analysis. Recently-discovered instabilities and flow structures are shown to be re-created in steady gas burners, allowing for more detailed studies, including statistical analysis made possible by the long time scales stationary flames can create. Correlations for the mean flame geometry, such as the flame tilt angle and flame length can also be obtained by these studies with appropriate nondimensional scaling.

Bibliography

[1] Mark A Finney, Jack D Cohen, Sara S McAllister, and W Matt Jolly. On the need for a theory of wildland fire spread. *International journal of wildland fire*, 22(1):25–36, 2013.

[2] Mark A Finney, Jason Forthofer, Isaac C Grenfell, Brittany A Adam, Nelson K Akafuah, Kozo Saito, et al. A study of flame spread in engineered cardboard fuelbeds: Part i: Correlations and observations. 2013.

[3] L Orloff, J De Ris, and GH Markstein. Upward turbulent fire spread and burning of fuel surface. In *Symposium (International) on Combustion*, volume 15, pages 183–192. Elsevier, 1975.

[4] P.H. Thomas. Some aspects of growht and spread of fire in the open. Vol. 40:pp. 139–164, 1967.

[5] Drysdale D.D. Wu Y. Atkinson, G.T. Fire driven flow in an inclined trench. Vol. 25:pp. 141–158, 1995.

[6] DA Smith. Measurements of flame length and flame angle in an inclined trench. *Fire safety journal*, 18(3):231–244, 1992.

[7] DD Drysdale and AJR Macmillan. Flame spread on inclined surfaces. *Fire Safety Journal*, 18(3):245–254, 1992.

[8] PJ Woodburn and DD Drysdale. Fires in inclined trenches: the dependence of the critical angle on the trench and burner geometry. *Fire safety journal*, 31(2):143–164, 1998.

[9] Ying Wu, HJ Xing, and G Atkinson. Interaction of fire plume with inclined surface. *Fire Safety Journal*, 35(4):391–403, 2000.

[10] J De Ris and L Orloff. The role of buoyancy direction and radiation in turbulent diffusion flames on surfaces. In *Symposium (International) on Combustion*, volume 15, pages 175–182. Elsevier, 1975.

[11] MJ Gollner, X Huang, J Cobian, AS Rangwala, and FA Williams. Experimental study of upward flame spread of an inclined fuel surface. *Proceedings of the Combustion Institute*, 34(2):2531–2538, 2013.

[12] Y Oka. Modelling of unconfined flame tilt in cross-winds int. assoc. of fire safety and science. In *Proceedings of the 6 th International Symposium on Fire*, pages pp. 1101–1112, 2000.

[13] Yasushi Oka, Osami Sugawa, Tomohiko Imamura, and Yoshiyuki Matsubara. Effects of cross-winds to apparent flame height and tilt angle from several kinds of fire source. In *Proceedings of the 7th International Symposium on Fire, International Association of Fire Safety and Science*, pages pp. 915–926, 2002.

[14] WMG Malalasekera, Henk K Versteeg, and K Gilchrist. A review of research and an experimental study on the pulsation of buoyant diffusion flames and pool fires. *Fire and materials*, 20(6):261–271, 1996.

[15] Hiroyuki Sato, Kenji Amagai, and Masataka Arai. Scale modeling of puffing frequencies in pool fires related with froude number. In *Progress in Scale Modeling*, pages 133–147. Springer, 2008.

[16] Anthony Hamins, Takashi Kashiwagi, and Robert R Buch. Characteristics of pool fire burning. *ASTM special technical publication*, 1284:15–41, 1996.

[17] Brittany A Adam, Nelson K Akafuah, Mark Finney, Jason Forthofer, Kozo Saito, et al. A study of flame spread in engineered cardboard fuelbeds: Part ii: Scaling law approach. 2013.

[18] Jason M Forthofer and Scott L Goodrick. Review of vortices in wildland fire. *Journal of Combustion*, 2011, 2011.

[19] William S Saric. Gortler vortices. *Annual Review of Fluid Mechanics*, 26(1):379–409, 1994.

[20] P Hall. The linear development of görtler vortices in growing boundary layers. *Journal of Fluid Mechanics*, 130:41–58, 1983.

[21] EM Sparrow and RB Husar. Longitudinal vortices in natural convection flow on inclined plates. *Journal of Fluid Mechanics*, 37(02):251–255, 1969.

[22] Kenzo Kitamura and Fumiyoshi Kimura. Heat transfer and fluid flow of natural convection adjacent to upward-facing horizontal plates. *International journal of heat and mass transfer*, 38(17):3149–3159, 1995.

[23] Peter Jeschke and Hans Beer. Longitudinal vortices in a laminar natural convection boundary layer flow on an inclined flat plate and their influence on heat transfer. *Journal of Fluid Mechanics*, 432:313–339, 2001.

[24] James M Wallace. Highlights from 50 years of turbulent boundary layer research. *Journal of Turbulence*, (13), 2012.

[25] Dan Jimenez, Mark A Finney, Jack Cohen, et al. Design and construction of gas-fed burners for laboratory studies of flame structure. *Notes*, 2010.

[26] L Audouin, G Kolb, JL Torero, and JM Most. Average centreline temperatures of a buoyant pool fire obtained by image processing of video recordings. *Fire Safety Journal*, 24(2):167–187, 1995.

[27] RF Blackwelder and RE Kaplan. On the wall structure of the turbulent boundary layer. *Journal of Fluid Mechanics*, 76(1):89–112, 1976.

[28] John F Foss and James M Wallace. The measurement of vorticity in transitional and fully developed turbulent flows. In *Advances in fluid mechanics measurements*, pages 263–321. Springer, 1989.

[29] Cohen Jack D Forthofer Jason A McAllister Sara S Adam Brittany A Akafuah Nelson K English Justin Saito Kozo Gorham Daniel J Gollner Michael J Finney, Mark A. Experimental evidence of buoyancy controlled flame spread in wildland fires. 2014.

[30] Baki M Cetegen and Tarek A Ahmed. Experiments on the periodic instability of buoyant plumes and pool fires. *Combustion and Flame*, 93(1):157–184, 1993.

[31] GM Byram. Combustion of forest fuels. in forest fire: control and use.(ed. kp davis) pp. 61–89, 1959.

[32] James G Quintiere. Scaling applications in fire research. *Fire Safety Journal*, 15(1):3–29, 1989.